3D microstructural architecture of deformed glacigenic sediments associated with large-scale glacitectonism, Jasmund Peninsula (NE Rügen), Germany

Anna Gehrmann[1*], Heiko Hüneke[1], Martin Meschede[1] and Emrys Phillips[2]

[1] Ernst-Moritz-Arndt-Universität Greifswald, Institut für Geographie und Geologie, Friedrich-Ludwig-Jahn-Straße 17a, D-17487 Greifswald (anna.gehrmann@uni-greifswald.de)

[2] British Geological Survey, Murchison House, West Mains Road, Edinburgh EH9 3LA, Scotland, UK

*corresponding author

Abstract

The Wissower Bach Syncline on the Jasmund Peninsula (NE Germany) has been examined to understand the complicated glacitectonic environment in the southern Baltic Sea region, comprising folds and thrust faults from the Weichselian Pleniglacial. Soft-sediment thin sections from a SW-dipping thrust fault at the southwestern limb of the syncline between Cretaceous chalk (hangingwall) and Pleistocene deposits (footwall) were analysed using micromorphology and microstructural mapping. Within the diamicton bounding the fault, three different clast microfabrics were distinguished: an older, but dominant S1 fabric; a second S2 foliation orientated perpendicular to S1; and a younger subvertical S3 fabric. These fabrics developed during large-scale folding and thrusting, subsequent fabric rotation adjacent to the thrust fault accompanied by dewatering of the diamicton and extension; the latter implying late-stage reactivation and gravitational relaxation at the southwestern limb of the syncline as the ice retreated. The combination of a 3D microstructural model and the macroscale information has led to the development of a detailed model for the evolution of the Wissower Bach Syncline during glacitectonism and the localised reactivation of the associated thrusts in response to ice retreat. Moreover, this methodology provides a robust dataset on which to interpret the structural evolution of glacitectonic complexes.

Keywords: Isle of Rügen, 3D microstructural architecture, microfabrics, glacitectonics, Weichselian Pleniglacial

Introduction

Large-scale glacitectonic deformation, resulting in locally significant disruption and shortening of both bedrock and sedimentary sequences, has been reported from a number of previously glaciated areas, including North America (e.g. Moran *et al*., 1980; Bluemle and Clayton, 1984), the United Kingdom (e.g. Harris *et al*., 1995, 1997; Thomas and Chiverrell, 2007; Phillips *et al*., 2008; Burke *et al*., 2009) and northern Europe (e.g. van der Wateren, 1986; van der Wateren *et al*., 2000; Huuse and Lykke-Andersen, 2000; Pedersen, 2005, 2014). The detailed analysis and interpretation of the structural features developed within these glacitectonic complexes, employing the techniques routinely used by structural geologists, has not only led to a more systematic approach to investigation of complicated polydeformed glacigenic sequences, but also provides important information on the character of these deformation events and their relationship to glacier/ice sheet dynamics (e.g. Benn and Evans, 1996; Pedersen, 2005, 2014; van der Wateren *et al*., 2000; Phillips *et al*., 2002; Lee and Phillips, 2008; Benediktsson *et al*., 2008; Phillips *et al*., 2008). Microstructural analysis, in combination with field macroscale studies, is also increasingly being used as a principal tool for investigating the progressive development of folds, faults and foliations resulting from subglacial and proglacial deformation (e.g. van der Meer *et al*., 2003; Menzies, 2000; Phillips and Auton, 2000; van der Wateren *et al*., 2000; Menzies *et al*., 2006; Phillips *et al*., 2007; Lee and Phillips 2008; Denis *et al*., 2010; Vaughan-Hirsch *et al*., 2013; Narloch *et al*., 2012, 2013), as well as investigating the role played by pressurised melt water during glacier induced deformation (Hiemstra and van der Meer, 1997; Baroni and Fasano, 2006; Phillips and Merritt, 2008; van der Meer *et al*., 2009; Denis *et al*., 2010; Phillips *et al*., 2012; Narloch *et al*., 2012, 2013).

Germany's largest island, the Isle of Rügen, located in the SW-Baltic Sea (Fig. 1a) is well-known for large-scale glacitectonic folding and thrusting (Groth, 2003; Müller and Obst, 2006; Ludwig, 2011), which is well-exposed in the steep sea cliffs along its eastern and southeastern coast (Fig. 1). This glacier-induced deformation affected not only the Pleistocene glacigenic sediments, but also the chalk bedrock and is widely considered to have occurred during the Weichselian (Devensian) glaciation of the region (Groth, 2003; Müller and Obst, 2006; Ludwig, 2011). The deformation structures on the Jasmund Peninsula in the NE of the Isle of Rügen (Fig. 1) have been intensively investigated for more than a century (Credner, 1892; Gripp, 1947; Bülow, 1955; Groth, 2003; Müller and Obst, 2006; Ludwig, 2011). Recent work by Groth (2003), Müller and Obst (2006), and Ludwig (2011) have provided a contradictory structural interpretation of the glacitectonic evolution of the peninsula.

Unravelling the complex deformation history recorded by the rocks and sediments of the Jasmund Peninsula, however, is critical to our understanding of ice sheet dynamics in this part of the Baltic Sea during the Weichselian (Devensian).

This paper presents the results of a detailed structural study of the polydeformed glacigenic sediments present within the core of the Wissower Bach Syncline on the Jasmund Peninsula (Figs. 1b and c). The combination of macro (field) and microstructural (micromorphology) techniques is used to investigate the processes active during large-scale folding of the Pleistocene sediments and chalk bedrock affected by the Wissower Bach Syncline. Orientated, large format thin sections of the diamicton exposed immediately adjacent to the contact with the folded chalk bedrock are used to investigate ductile shearing along this major lithological/rheological contact and to construct detailed models of the 3D fabric geometries developed within these sediments. This information is used to develop a progressive deformation model for large-scale fold development in this part of the Jasmund Peninsula and relating it to ice sheet dynamics. The combination of a 3D microstructural analysis and the macroscale information gives rise to a detailed model of the evolution of this glacitectonic complex and provides new information, which is not recognisable at macroscale.

Location of the study area and its geological setting

The Wissower Bach Syncline (see Steinich, 1972), the focus of this study, is situated on the southeastern coast of the Jasmund Peninsula, 1.5 km northeast of Sassnitz on the Isle of Rügen (Fig. 1). It is exposed in a c. 200 m wide and 40 m high section of sea cliffs (Fig. 2). This syncline (axial surface dips to the SW, 200-250/45-50) is one of a number of large-scale folds and associated thrusts which form an imbricate thrust stack, or duplex, deforming both the Upper Cretaceous (Maastrichtian) chalk bedrock and overlying unconsolidated Pleistocene glacigenic deposits (Credner, 1892; Gripp, 1947; von Bülow, 1955; Groth, 2003; Ludwig, 2011). The large-scale and structural characteristics of the Jasmund thrust-fold complex are comparable to many of the large glacitectonic complexes described in areas of former glaciated terrain, such as Møns Klint in SE Denmark (Pedersen, 2000; Pedersen and Gravesen, 2009; Pedersen, 2014).

The glacial deposits exposed at the Jasmund study area have been subdivided into at least three tills (M1 to M3) with intercalated units (I1 and I2) comprising gravel, sand and clay. The regional stratigraphic correlation of the individual tills and their relationships to the interbedded sediments is still under debate (see Kenzler *et al.,* 2015 and references therein). The older M1 till is widely thought to have been deposited during the Saalian (Wolstonian) glaciation (Marine Isotope Stage (MIS 6) (Panzig, 1995; Müller and Obst, 2006) and is interpreted as a subglacial traction till (Evans *et al*., 2006). No unequivocal Eemian aged sediments (MIS 5e) have been identified in the Jasmund cliff sections (Steinich, 1992; Ludwig, 2006). The majority of the Pleistocene sedimentary record (I1, M2, I2 and M3; Fig. 2) of the Jasmund Peninsula is considered to have been laid down during the Weichselian glaciation when the Scandinavian Ice Sheet extended southwards across the Baltic Sea and into northern Europe. In this part of the Baltic Sea the Weichselian glaciation has been divided into three ice advances; the Brandenburg/Frankfurt phase (W1, oldest), the Pomeranian phase (W2) and finally the Mecklenburg phase (W3, youngest) (Katzung and Müller, 2004; Müller, 2004; Litt *et al.*, 2007; Janke and Niedermeyer, 2011). These three phases resulted in the deposition of regionally extensive till sheets intercalated by interstadial sediments (Groth, 1969; Ludwig, 2005; Müller and Obst, 2006; Panzig, 1995; Janke and Niedermeyer, 2011). While the M2 till at Jasmund has been assigned to the Brandenburg/Frankfurt W1 phase, the age of the M3 till is poorly constrained and has previously been correlated with either the Pomeranian W2 ice advance, or locally the Mecklenburg W3 phase. If the regional correlations are correct, it would suggest that the formation of the glacitectonic complex of Jasmund post-dated the deposition of the M2 diamicton and the I2 sands and gravels, and therefore the Brandenburg/Frankfurt W1 advance phase. Consequently, glacitectonism of the Jasmund Peninsula probably occurred after the Last Glacial Maximum (MIS 2), with large-scale folding and thrusting occurring in response to a re-advance of the Scandinavian Ice Sheet during the Pomeranian W2 phase (around 18.5 – 16.0 ka) (Groth, 2003; Müller and Obst, 2006).

One striking feature of the Jasmund Peninsula seen on the digital elevation model (DEM) of the area is the sequence of SW-NE-trending ridges in the southern part of the region (southern structural complex), and approximately NW-SE-trending landforms in the north (northern structural complex) (Fig. 1c). Given that deposits relating to the Mecklenburg W3 phase are only locally preserved/developed, if at all, it can be argued that these landforms are also related to the Pomeranian W2 phase ice advance. Previous workers (Credner, 1892; Gripp, 1947; von Bülow, 1955; Groth, 2003; Ludwig, 2011) have divided the Jasmund glacitectonic complex into northern and southern zones, with these structural “domains” broadly corresponding to landform assemblage zones observed on the DEM (see Fig. 1c). Ludwig (2011) has suggested that the Jasmund glacitectonic complex, which includes the Wissower Bach Syncline, developed at the confluence of two major ice streams which were active during the Pomeranian W2 phase. In this model, the Jasmund Peninsula would have formed a topographic high or nunatak which at least initially separated the Baltic ice into two ice streams. Pressure formed between the two competing flows resulted in folding and thrusting of the chalk bedrock and its Pleistocene cover, as well as the formation of the associated landforms (composite ridges) as the peninsula was progressively inundated by ice from both the northeast and southeast (see Fig. 1c).

Methods

The structural architecture of the Wissower Bach Syncline and the deformation history recorded by glacial sediments and pre-glacial chalk bedrock exposed on the limbs of this major glacitectonic structure, have been investigated using a range of macroscale techniques. The section was described on the basis of its macroscale features with particular emphasis being placed on recording the type of bedding, sediment-type, bed geometry and structure (both sedimentary and glacitectonic). The orientation of the bedding planes on both limbs of the fold, the main fault, and flint bands within the hangingwall were recorded from a number of points along the length of the section (dip direction/dip). These data were plotted on lower hemisphere stereographic projections (Fig. 3) using the open source software OpenStereo (Grohmann and Campanha, 2010). These data were integrated with previously published information from the area (Steinich, 1972). Overlapping photographs were taken of the cliff (at a distance of 500 m from the cliff face) enabling the analysis of the larger-scale syncline (Fig. 2). Additionally, the digital elevation model (DEM) of Jasmund (Fig. 1c), which is based on LiDAR data provided by the LAiV M-V, has been consulted to place the results from the microstructural mapping and the local macroscopic structural investigations at the Wissower Bach Syncline within the broader context of regional ice sheet dynamics.

The chalk at the glacitectonised boundary and the underlying diamicton were sampled for detailed microstructural analysis. Prior to sampling the sections at both sites were logged, photographed and described in detail (Fig. 4) with particular emphasis being placed on recording the macroscale variation in lithology and structure of the diamictons. In order to examine the range of microstructures developed associated with the partitioning of deformation along this glacitectonised boundary two orientated blocks (JA03, JA04) were collected; (i) sample JA03 includes the boundary between the chalk and diamicton enabling deformation within the bedrock to be directly compared with the adjacent diamicton; and (ii) sample JA04 is of the apparently massive diamicton approximately 10 cm below this contact (Fig. 2 inset b). The samples were taken using 10 cm cubed Kubiena tins which were cut (using a knife) into the face in order to limit sample disturbance (see van der Meer, 1993; Menzies, 2000). The position of the sample within the glacigenic sequence, its orientation relative to magnetic north, depth and way-up were marked on the outside of the tin during collection. Each sample was then removed from the face and stored in a drying furnace (c. 25 °C) for at least two weeks to get rid of pore water residues in a gentle way prior to sample preparation.

Samples were impregnated involves the impregnation with polyester resin and stored in a vacuum drying oven (c. 25 °C, 700-800 mbar) for c. two weeks, then six weeks outside the oven, hence allowing the resin to cure. Large format orientated thin sections were taken from the centre of each of the prepared samples, thus avoiding artefacts associated with sample collection. Three mutually perpendicular thin sections were cut from each sample to allow the detailed examination of the microstructures in 3 dimensions (see Phillips *et al.*, 2011). The thin sections were examined using a petrological microscope with the terminology used to describe the various microtextures following that proposed by van der Meer (1987, 1993) and Menzies (2000). Detailed microstructural maps and quantitative data for the clast microfabrics developed within the diamicton layers were obtained using the methodology of Phillips *et al*. (2011) (also see Vaughan-Hirsch *et al*., 2013; Phillips *et al*., 2013). This microstructural mapping approach was used alongside existing methods of analysis resulting in the detailed microstructural and sedimentological analysis of the glacigenic sediments. Plotting of the orientation data obtained for the long axes of fine sand to pebble sized clasts (skeleton grains) within the diamictons on rose diagrams was carried out using the open source software OpenStereo (Grohmann and Campanha, 2010). Successive generations of fabrics (S1, S2, …Sn) are distinguished by the nomenclature normally used in structural geological studies (S1 earliest fabric to Sn latest). However, this nomenclature does not necessarily imply that these structures were developed in response to separate deformation events (D1, D2, ...Dn).

Sedimentary sequence and macroscale deformation structures

The Wissower Bach Syncline (54°31. 923' N, 13°40.697' E) preserves a comprehensive Pleistocene sedimentary record that is representative for the southern structural domain of Jasmund. It is bounded at its base by an angular unconformity with a very low angle of discordance, truncating the Maastrichtian chalk. The Pleistocene succession is most clearly exposed and studied at the northeastern limb of the syncline, where it has been divided into M1, I1, M2, I2 and M3 units (Figs. 2 and 4) (adapted from Jaekel, 1917).

At the base of the sequence, the **M1** diamicton para-conformably overlies the chalk (Figs. 2 and 4 (see inset c)). This dark grey to red-brown (at top of unit), sandy to gravelly diamicton (c. 2.5 m thick; Fig. 4) is well jointed and possesses a clayey to silty matrix. The gravels and coarse sands are predominantly composed of Palaeozoic limestone as well as granite and gneiss. Boulder-sized clasts comprising granite and gneiss are only a minor component and appear to be concentrated at the base of the diamicton where it also contains stringers or streaks of deformed chalk derived from the underlying bedrock. M1 also contains a number of light grey, lenticular, channel-like units composed of clast-supported gravel containing cobbles of limestone and crystalline rocks in a silt/clay matrix. The composition of the gravel is comparable to the M1 diamicton, the key difference between the two sediments being their depositional fabric.

The M1 diamicton is conformably overlain by a composite sequence (**I1**) of sands and gravels including a 2 m thick unit of clay. The sand unit representing the lower part is 2.5 to 3 m thick and preserves an overall fining-upwards sequence (Fig. 4). At its base, a clast-supported cobble layer (clasts c. 10 to 15 cm diameter) occurs with a brown, silty to fine-grained sand matrix. It is directly overlain by a bedded sequence of light brown to white, parallel-laminated, fine-grained sand containing thin interbeds of medium-grained sand with scattered clasts of coarse sand to fine gravel. Additionally, the sands contain out-sized boulders (up to 30 cm in diameter) of crystalline rocks (gneiss, granite), which are concentrated within a discrete layer or lens at a height of c. 4 m above the base of the cliff (Fig. 4). The lower part of the sandy sequence is interrupted by a folded layer (c. 20 cm thick) of brown-grey clay. Above this deformed layer, however, I1 is undisturbed and composed of cross- to ripple-laminated, fine-grained sand (see Fig. 4), intercalated with several brown-grey coloured silt/clay layers (c. 5 cm thick). The sands are locally oxidised resulting in a yellowish to red-brown stain (see Fig. 4 inset b).

The fining upward sand unit is overlain by a c. 2 m thick grey clay (Fig. 4). On the northeastern limb of the syncline, the lower part of the clay unit is light grey in colour and possesses a fine lamination. This passes upwards into a c. 90 cm thick layer of grey-brown clay. However, on the southwestern limb this lamination is absent. Large out-sized clasts locally occur, and range from coarse sand to gravel, as well as rare cobbles. The clays are directly overlain by a second unit of light brown, fine-grained sands (Fig. 4). This upper I1 sand is much thinner than the lower sand and appears to be laterally discontinuous, possibly being cut out by the base of the overlying M2 diamicton.

The I1 deposits are in turn overlain by a 10 to 15 m thick massive, grey-brown diamicton, **M2** (Fig. 4), which forms the core of the Wissower Bach Syncline (Fig. 2). This diamicton has a silty matrix and contains relatively common coarse gravel to boulder sized clasts, mainly comprising granite, gneiss and limestone. A number of gravel and sand lenses are also present. In detail the M2 diamicton can be divided into two (see Ludwig, 1964;

Panzig, 1995): (i) a lower, clast-poor M2α (m2-2u) subunit which is grey-blue to grey-brown in colour with a clayey matrix; and (ii) an upper, more clast-rich, sandy M2β (m2-2o) diamicton.

The **I2** sands and gravels form a narrow (1 to 2 m thick; Fig. 4) poorly exposed unit within the core of the Wissower Bach Syncline (Fig. 2). These sediments occur near the upper rim of the cliff section and were not accessible for detailed analysis.

At the top of the cliff section the Wissower Bach Syncline is truncated by the erosive base of the later **M3** sedimentary complex (Figs. 2 and 4). This light grey-brown, sandy diamicton contains large boulders of crystalline rocks, as well as a very high proportion of flint clasts and deformed stringers or streaks of chalk. It is characterised by internal folds and interfingering of light brown and darker streaks. Additionally, the M3 diamicton contains lenticular, channel-like features (mainly at its base) filled by stratified coarse cobble and gravel (Fig. 4 inset a), comprising crystalline rocks and flint.

The lithostratigraphic units **M1** and **M2**, which are both characterized by diamictic lithologies, are interpreted as till units mainly formed by traction (lodgement and deformation) and more rarely by melt-out in a subglacial environment. The M1 till includes rafts of glacitectonised chalk and covers a boulder pavement, which is an erosional lag deposit predating the deposition of the M1 till.

The composite **I1** unit comprises glacifluvial and glacilacustrine deposits. The fining-upward sequence within the lower part of the unit indicates an accumulation mainly controlled by the melting and retreating M1 glacier. Clay beds are formed at quieter conditions (standing water) and during low sediment input. Out-sized clasts and boulders of crystalline rocks are interpreted as dropstones derived from melting brash ice or icebergs. The sediments of the poorly exposed I2 unit are primarily formed by glacifluvial accumulation, which can be derived from coeval deposits in neighbouring outcrops at the sea cliff.

The (inaccessible) **M3** sedimentary complex includes a subglacial traction till. Parts of the diamictic sediments, however, may have been formed by debris flows supplied from the raised chalk ridges. This is indicated by the high amount of locally-derived materials such as chalk and flint pebbles. The channel fills at the base of the unit are interpreted as (subglacial) melt-out deposits.

The M3 unit exposed at the upper cliff margin is preserved as an undisturbed, horizontally stratified succession, whereas the older sedimentary record, cropping out below the base-M3 disconformity, is structurally deformed (Fig. 2). In the NE part of the studied cliff section, the chalk and the overlying record consisting of units M1 to I2 form a paraconform succession dipping to the SW. Its stratigraphic younging direction is upward and towards SW. In the SW part of the cliff section, the succession from M1 to I2 is still dipping to the SW but overturned (Figs. 2 and 3d) as indicated by inverted syn-depositional sedimentary structures and other way-up criteria. In this part of the outcrop, the younging direction is downward and towards NE, which is recognized by the lithostratigraphic order and the fining-up of the lower I1 sequence. Consequently, the Cretaceous chalk and the Pleistocene M1-to-I2 record display a NE-verging syncline that is truncated at the base of the M3 unit. The fold closure is located within the I2 unit.

The NE-verging Wissower Bach Syncline is very tight to isoclinal, moderately inclined, and deforming both the Upper Cretaceous (Maastrichtian) chalk bedrock and unconsolidated pre-M3 Pleistocene glacigenic deposits (Fig. 2). The northeastern limb is orientated at c. 247/50 SW and is the right-way-up (Fig. 3) with the Pleistocene glacigenic sequences resting paraconformably upon Maastrichtian chalk bedrock. Primary bedding within the chalk is preserved by laterally extensive flint bands (Fig. 2) and dips to SW (250/45 SW; Fig, 3b). On the southwestern limb of the fold (c. 203/44 SW; Fig. 3a), on contrary, this sequence is overturned/inverted (Figs. 2 and 3d). The former lithostratigraphical boundary between the chalk and the Pleistocene record has been modified by a SW/WSW-dipping (260/50 WSW; Fig. 3c) reverse fault. This fault produced a sharp to wavy boundary marked by a thin glacitectonite composed of chalk and streaks/stringers of the M1 diamicton (see Fig. 2 inset a). The core of the syncline is largely obscured by debris (Fig. 2); the hinge of this fold occurs below sea level. No small- and/or meso-scale parasitic folding of either the chalk or glacial sediments have been recognised associated with the large-scale syncline at Wissower Bach (see Fig. 2).

The Wissower Bach Syncline is a NW-SE trending structure. It is located within the southern structural domain of Jasmund, which is dominated by a series of SW-NE-trending ridges (Fig. 1c) turning into a WNW-ESE trend close to the studied coastal cliff section (see Fig. 1). These composite ridges reflect the “structural grain” of the underlying glacitectonised Pleistocene sediments and chalk bedrock.

Micromorphology and microstructural analysis

Two samples of the M1 diamicton exposed on the overturned SW-limb of the Wissower Bach Syncline were taken for micromorphological and microstructural analysis: (i) sample JA03 includes the faulted and tectonised contact between the chalk and the diamicton; and (ii) the lower sample JA04 is located within the M1 diamicton approximately 10 cm below the fault boundary (see Fig. 2 inset b). A number of thin sections were prepared from each sample (sample JA03: x4 vertical thin sections JA03.1, JA03.2, JA03.3, JA03.4 and x2 horizontal sections J03.5, JA03.6; and sample JA04: x3 vertical sections JA04.1, JA04.2, JA04.3 and x1 horizontal section JA04.5) to enable the relationships between the various microstructures and clast microfabrics developed within the diamicton to be examined in three dimensions. The range of microstructures observed within the diamicton and chalk are shown in figures 5 and 6. Representative microstructural maps of a number of thin sections are illustrated in figures 7 to 12.

Micromorphology of the M1 diamicton and chalk

In thin section the M1 diamicton is composed of apparently massive, relatively fine-grained, matrix-supported sand with a grey-brown silty-clay matrix (Fig. 5). The coarse silt to sand-grade clasts (skeleton) are predominantly sub-angular to angular in cross-section with a low sphericity (Fig. 5a, b c and d). However, subrounded to well-rounded grains are also present (Figs. 5e and f) with the rounded nature of these polycyclic clasts probably being inherited from the source rock/sediment. The clasts are mainly composed of monocrystalline quartz as well as subordinate amounts of polycrystalline quartz and feldspar. The larger detrital grains (>500 µm) also include plutonic igneous (granite) and sedimentary (limestone) lithic (rock) fragments (see Figs. 5c to f).

Arcuate and roughly circular alignments and clusters of sand grains are locally present within the diamicton (Figs. 5a and b) and are interpreted as turbate structures formed in response to ductile deformation (c.f. van der Meer, 1987, 1993; Menzies, 2000). Locally, these structures enclose the larger lithic clasts (Figs. 5e and f); the latter forming a “core stone” to these rotational deformation features. Other deformation structures present include linear grain alignments and shears (Figs. 5c and d), and rare crushed grains (Fig. 6f); the latter being relatively more abundant in the sample JA04. In general, the matrix to the diamicton shows very little evidence of deformation. However, a weak plasmic fabric, defined by optically aligned clay minerals, is locally apparent. The weak nature of this foliation may simply reflect the low modal proportion of clay minerals and/or presence of very fine-grained (micritic) carbonate (e.g. calcite) within the matrix to the diamicton, rather than the relative intensity of deformation/fabric development.

The boundary between the M1 diamicton and structurally overlying chalk is sharp, but irregular in nature (Fig. 6a and b, also see Fig. 7). In detail this lithological boundary is highly involute and deformed by small flame-like structures (Figs. 6a and b) as well as poorly developed disharmonic folds (Fig. 6d). Thin stringers of fine-grained (micritic) carbonate were locally observed extending from the chalk-diamicton contact into the adjacent glacigenic sediment (Fig. 6e) where they appear to be lining small-scale shears. Small, S-shaped to sigmoidal augen of diamicton (Figs. 6a and b), possessing elongate tails in some places (Fig. 6c), can occur in the chalk. The shape of these structures locally records a dextral (top to right) sense of rotation consistent with a northerly directed (in this plane of section) sense of shear (Fig. 6b). The presence of augen of diamicton within the chalk as well as thin stringers of carbonate within the M1 diamicton provide clear evidence that the deformation along this lithological boundary led to the localised 'mixing' of these two lithologies. Although deformed, the chalk immediately adjacent to the contact contains shell fragments, bryozoans, echinoderm spines and foraminifera (50 to 100 µm size). Importantly the delicate, thin walled tests of the foraminifera are intact (unbroken) suggesting that the intensity of deformation accommodated by the chalk was relatively low. The chalk is mainly composed of very fine-grained, dusty-looking grey-brown carbonate. However, immediately adjacent to the contact with the M1 diamicton it also contains angular to subangular sand grains (Fig. 6c) providing further evidence for at least some mixing of the chalk with the sandy diamicton during deformation.

3D microstructural analysis

Detailed mapping of the microstructures within the thin sections taken from samples JA03 and JA04 has revealed that they possess three main generations of clast microfabrics (S1 (oldest) to S3 (youngest); Figs. 7 to 12) defined by the preferred shape alignment of elongate coarse silt and sand grains present within the diamicton. Importantly, the orientation, geometry and spatial relationships of these three microfabrics are broadly similar in both samples indicating that they have encountered the same overall deformation history. The mutually perpendicular thin sections taken from each of the samples (Sample JA03 - JA03.2, orientation S-N (Fig. 7); JA03.3, orientation W-E (Fig. 8); and JA03.6, subhorizontal (Fig. 9); Sample JA04 - JA04.1, orientation S-N (Fig. 10); JA04.3 orientation W-E (Fig. 11); and JA04.5, subhorizontal (Fig. 12) have enabled these fabrics to be examined in three dimensions. The resultant three-dimensional model of the microfabric system at the tectonic chalk-diamicton contact is illustrated in Fig. 13.

The dominant foliation in both JA03 and JA04 is the **S1 fabric** (see rose diagrams on Figs 7 to 12), a discontinuous, heterogeneously developed (see Figs. 7 and 9) planar to anastomosing fabric defined by short (JA03; Fig. 7) to elongate (JA04; Fig. 10), closely to moderately spaced microfabric domains. In both JA03 and JA04, the northerly dipping S1 can be divided into two sub-fabrics: (i) a gently inclined S1a foliation (dark blue on Figs. 7 to 12);

and (ii) a more steeply dipping and more pervasively developed S1b fabric (pale blue on Figs. 7 to 12). In detail, the relative intensity of both these early foliations increases structurally downwards from sample JA03 and into JA04 (compare Figs. 7 and 10, also see Fig. 13); indicative of an apparent increase in the intensity of deformation, which led to the imposition of S1 away from the chalk-diamicton boundary. 3D analysis of the microfabrics has revealed that this increase in the relative intensity of S1 is accompanied by an anti-clockwise rotation (c. 70° to 90°) in the direction of dip of this fabric (Fig. 13). Adjacent to the chalk-diamicton boundary, in sample JA03, S1 dips at a moderate angle towards the NW (S1a - 307/48 NW; S1b - 307/55 NW; Fig. 13). Furthermore, a comparable north-westerly dipping foliation, coplanar to S1 within the adjacent diamicton, is developed within the adjacent chalk where it is defined by the preferred alignment of elongated bioclasts (Figs. 7 and 8). In contrast, in sample JA04 S1 dips to NE (S1a - 042/20 NE; S1b - 042/54 NE; Fig. 13).

S1 is cross-cut, and locally deformed, by a later **S2 fabric** defined by variably spaced, irregular to continuous domains (Figs. 7 to 12). The spacing of these domains is highly variable, reflecting the heterogeneous/patchy development of S2 within the M1 diamicton. The earlier S1 fabric is preserved within the microlithons separating the S2 microfabric domains where it is deformed by small-scale microfolds or crenulations; the axial surfaces of these folds appear coplanar to the adjacent S2 fabric. The relatively younger S2, therefore, takes the form of a moderate to widely spaced, planar to anastomosing weakly developed crenulation cleavage (e.g. JA03.2; Fig. 7). Locally the earlier formed S1 fabric is dislocated or offset across the S2 fabric, implying an apparent normal sense of movement with downthrow towards the south (Fig. 7 and 10). In both JA03 and JA04, the southerly dipping S2 can be divided into two sub-fabrics: (i) a steeply inclined S2a foliation (dark green on Figs. 7 to 12); and (ii) a more gently dipping S2b fabric (pale green on Figs. 7 to 12). The relative age relationship(s) between these two sub-fabrics is uncertain. However, locally S2b appears to cross-cut the potentially earlier S2a fabric (see Fig. 10). As with the S1 fabric, the relative intensity of S2 increases downwards from sample JA03 and into JA04, away from the chalk-diamicton boundary (compare Figs. 7 and 10). The S2 domains occur orthogonal to S1 and in 3D clearly define a southerly plunging linear fabric (Fig. 13). In sample JA03, adjacent to the chalk-diamicton boundary, S2 is moderately inclined to SE (S2a - 136/49 SE; S2b - 136/31 SE; Fig. 13). Whereas, in sample JA04, S2 plunges towards the SW (S2a - 214/44 SW; S2b - 214/68 SW; Fig. 13). Consequently, as with S1, the S2 linear fabric shows a pronounced anti-clockwise rotation in orientation with decreasing distance to the chalk-diamicton boundary (see Fig. 13).

Both S1 and S2 are cross-cut by the relatively younger **S3 fabric** (Figs. 7 to 12). This widely to moderately spaced foliation is defined by steeply inclined to subvertical (JA03 - 176/85 S; JA04 - 181/90 S; Fig. 13), irregular to anastomosing, discontinuous domains (Figs. 7 to 13). In contrast to both S1 and S2, the relative intensity of S3 appears to increase towards upwards the chalk-diamicton boundary (compare Figs. 7 and 10) and shows a relatively consistent orientation in both samples.

Discussion and Interpretation

The results of the detailed microstructural mapping and 3D analysis of the deformation structures developed within the M1 diamicton presented here clearly demonstrate the potential benefits of this type of analysis when applied to glacitectonically deformed sequences. The presence of a large scale syncline and associated thrust fault deforming the chalk and overlying glacigenic sediments exposed at Wissower Bach has been known for some time (e.g. Steinich, 1972). The present 3D microstructural analysis has now provided further information regarding the development of these glacitectonic structures, which are not recognisable in the field. This includes: the partitioning of deformation into the relatively weaker unconsolidated diamicton during folding leading to the development of Riedel shears (stage 1); followed by the imposition of a second (S2) crenulation fabric as deformation continued (stage 2); the anti-clockwise rotation of the S1 and S2 microfabrics (stage 3); and finally the dewatering of the diamicton and imposition of S3, which apparently accompanied the localised reactivation of the earlier formed S2 fabric to form small-scale normal faults and extensional shears (stage 4).

Several previous studies have demonstrated that the combination of macro- and microstructural analyses enable a detailed model of the complicated deformation histories recorded by glacial sediments to be established (e.g. van der Meer *et al*., 2003; Menzies, 2000; Phillips and Auton, 2000; van der Wateren *et al*., 2000; Menzies *et al*., 2006; Phillips *et al*., 2007; Lee and Phillips, 2008; Denis *et al*., 2010; Vaughan-Hirsch *et al*., 2013; Narloch *et al*., 2012, 2013). However, these studies have been carried out on orientated thin sections cut parallel to the regional ice movement direction and are therefore only 2D in nature, different from this study.

Two different evolutional models were considered to describe the microstructures developed within the M1 diamicton and the chalk. The macroscopic basis of the first model is an antiformal stack produced by SW-directed thrusting, while the second model considers the already established syncline as part of a proximal imbricate fan that requires NE-directed thrusting and subsequent gravitational relaxation.

The **first evolutional model** for the glacitectonism at the Wissower Bach is discussed in Fig. 14. The development of an antiformal stack in the southern structural complex of Jasmund is assumed, which evolved from an ice push from NE. In the first stage (Fig. 14a) a fault-bend fold is formed along a primary ramp, dipping to NE. The second stage (Fig. 14b) is characterised most likely by a continued push from NE and progressive deformation. This leads to another fault-bend folding along a new ramp resulting in an antiformal stack (Fig. 14b). On the southwestern side of the stack, the thrust sheet is moved downwards along a normal fault dipping to SW, which may represent the fault at Wissower Bach.

This model could explain the normal faults at micro-scale (Fig. 10). Additionally, the macroscopic S-inverted folds within the chalk north of the Wissower Bach (Fig. 2, profile meters 200 to 250 in the cross section) may indicate an antiformal stack, due to a sort of drag folding along another SW-dipping normal fault in the lower part of the stack.

The **second evolutional model** considers the formation of an imbricate fan by ice push from SW as shown in Fig. 15. The documented Wissower Bach Syncline is interpreted as part of a footwall-thrust sheet below a SW-dipping ramp (Fig. 2). The SW-dipping fault bounding the syncline at its southwestern limb may represent one of the successive thrust-fault splays that branched up from a décollement surface at some depth below sea level.

Based on this model, the microstructural evolution of the M1 diamicton at the southwestern limb of the Wissower Bach Syncline can be explained by a series of events resulting from glacitectonically induced reverse- to thrust-faulting as outlined in more detail below. The youngest microfabric, on contrary, is attributed to normal faulting (inversion) due to gravitational relaxation and pore-water escape.

Concerning our current data base, we **favour the second evolutional model** (Fig. 15). The Pleistocene sediment record indicates a syncline, which must have been cut by a thrust fault at the southern limb. All faults along the coastal transect of the southern sub-complex dip south-westward or southward. In case that all these faults would represent a foreland dipping ramp, as assumed for the model 2, an extremely thick pile of an antiformal stack might be the consequence. The glacitectonic complex must have had a height of about 2 km, which is enormous and less realistic. Furthermore, there is a clear trend from south to north favouring model 1: the faults show a decreasing inclination (see Steinich, 1972), which can be interpreted as a stepwise steepening of the older faults (proximal, SW) due to the propagation of the active fault towards the foreland (distal, NE) as described by Pedersen (2005) for glacitectonic complexes. Consequently, an ice push from a southern source forming the folds and faults of the southern structural complex (Fig. 1c) is much more plausible than the formation of an antiformal stack by a straight push from NE. In addition, the digital elevation model (Fig. 1c) shows two arcuate sub-complexes that point to two deformation events including an ice push from both NE and SE. Thus, especially the southern sub-complex concave to SE has a much more complicated deformation history than the northern one. This makes the interpretation of the Wissower Bach structure to a bigger challenge.

Based on the interpretation that the faulted Wissower Bach Syncline is part of an NE-verging imbricate fan (model 2), the **microstructural evolution** of the M1 diamicton at the southwestern limb of the syncline can be divided into four stages. This reconstruction takes into account, that the sediment preferentially records the processes of the last deformation events (see Phillips et al. 2011). Thus, all the previous fabrics, in this case formed during the Saalian glaciation and superimposed during the ice advance of the Brandenburg/Frankfurt phase (W1), have been erased.

The **first evolutionary stage** led to the imposition of the **S1 fabric** (dip to NE) (Fig. 15a). The microfabric domains represent a downward movement of clasts into a general northerly direction on planar tracks. The geometry of this clast-fabric can be interpreted as Riedel shears with the S1 fabric representing the synthetic *R shears* recording narrow zones of extension and kinematically corresponding to normal "faults" (Fossen, 2010). It has to be taken into account that the S1 domains represent planes (cf. Fig. 13) that are generated by the clast long axes whose orientation can vary in two dimensions (more or less freely). In contrast, in a linear fabric system, the clast long axes are more restricted (axes are more or less sub-parallel), which is typical of the *P shears* (cf. Fig. 15a) that correspond to reverse "faults" (Fossen, 2010) and represent zones of compression. Such P shears, in this case perpendicular to S1, could also be established by microstructural mapping. Apparently, these are shear lines (**S2 fabric**) built together with the S1 domains, when the compressional stress acted from a general southerly direction.

During the **second evolutionary stage** (Fig. 15b), continued deformation led to the crenulation of **S1** (dip to NE) and imposition of **S2 (**dip to SW). The S1 fabric has been turned into folds with axial surfaces coplanar to the adjacent S2 fabric.

Continued deformation during the **third evolutionary stage** led to the modification and reorientation of the microfabrics present within the M1 diamicton (Fig. 15c). This reactivation led to the anti-clockwise rotation of both S1 and S2 within the fault zone so that the dip of S1 was changed from NE into NW and the plunge of S2 from SW into SE (see Fig. 13).

The **fourth evolutionary stage** is characterised by the development of the sub-vertical, planar **S3 fabric** (Fig. 15d). The domains defining this foliation could be interpreted as steeply inclined shears, or alternatively as an anastomosing sub-vertical foliation developed in response to dewatering of the diamicton. If we consider the steep shears to be a part of the Riedel shear zone, they can be interpreted as *R'-fractures*. However, the irregular to anastomosing nature of S3 is considered to be more consistent with this foliation having developed in response to the flow of escaping pore water and dewatering of the diamicton during the later stages of deformation. In this interpretation the S3 domains represent anastomosing conduits or fluid pathways taken by the escaping pore water. This can be confirmed by the character of the contact between the chalk and the diamicton at both macro and microscale, which shows a ductile structure and interfingering of both depositional units by porewater movement (see Fig. 6).

Also during the fourth stage, the S2 foliation has been reactivated and enhanced. Locally, it displays normal (extensional) faults which cross-cut and dislocate the earlier developed S1 domains (Fig. 15d; see Figs. 7 and 10). This microstructural relationship records a generally south-directed extension during possibly the later part of the proposed polyphase deformation history recorded by the M1 diamicton.

The results of the microfabric analysis outlined above have **implications** for late Weichselian ice-sheet dynamics and the development of regional-scale faulting during glacitectonism of the Jasmund Peninsula. After the ice advance of the Brandenburg/Frankfurt stage (W1), the Baltic Ice Stream advancing from NE is considered to have split into northern and southern branches around a topographic high or nunatak in the area now occupied by the Jasmund Peninsula (see Panzig, 1995; Ludwig, 2011). The southern branch of this ice stream is thought to have been responsible for the large-scale glacitectonic folding and thrusting on the southern side of the peninsula (southern structural complex, see Fig. 1c), including the Wissower Bach Syncline. The series of NE-SW trending ridges seen on the DEM of the region represents the surface expression of this folded and thrusted imbricate fan, and clearly demonstrates that the ice responsible for this glacitectonism advanced onto the Jasmund Peninsula from SE (Fig. 1c) (see Steinich, 1972). Compression directed from SE to NW generated by the advancing ice resulted in the folding and thrusting of both the chalk bedrock and overlying glacigenic sediments, leading to the early stages of the development of the Wissower Bach syncline (**first stage** with local pressure directed to NE, Fig. 15a). These initial stages of the development of the syncline were accompanied by flexural slip along the lithological boundary between the chalk and the diamicton, and the imposition of the S1 microfabrics within M1 (sample JA04). Movement along the boundary between the chalk and adjacent glacial deposits appears to have been partitioned into the relatively weaker, unconsolidated M1 diamicton; a conclusion supported by the preservation of delicate microfossils (e.g. foraminifera) within the chalk (sample JA03) exposed immediately adjacent to this glacitectonised contact.

The progressive development of the Wissower Bach Syncline in response to continued compression (**second stage**, Fig. 15b) is thought to have led to the further tightening of this syncline. The tightening of the fold may have accompanied the overturning and localised thrusting on the southern limb of the syncline. On a smaller scale, continued deformation resulted in the microscale folding (crenulation) of the earlier developed S1 fabric and imposition of the second foliation (S2) within the M1 diamicton.

During the **third stage**, ice is interpreted to have overridden a part of the Jasmund Peninsula, indicated by the erosional unconformity and the overlying sediment complex M3 (see Fig. 2, Fig. 15c). The orientation of the axial surface of the Wissower Bach Syncline coupled with the dip and strike of the S1 and S2 microfabrics developed within the M1 diamicton are consistent with a SW compression during at least the first and second stages of the proposed deformation model. However, the results of the 3D microstructural study clearly demonstrate that both S1 and S2 appear to have rotated (Fig. 15c) as deformation progressed, suggesting that there was a change in the orientation in stress regime being imposed by the overriding ice. Even though in general S1 dips towards the north and S2 to the south, there is a marked change in the orientation of these fabrics between sample JA03, located immediately adjacent to the chalk-M1 contact, and sample JA04, which occurs 10 cm below this tectonised boundary. In sample JA03, S1 is inclined to NW, whereas in JA04 it dips towards the NE. A similar apparent anti-clockwise rotation in the orientation of the clast microfabrics close to the chalk-M1 boundary is revealed by S2 (JA03: dip to SE, JA04: dip to SW). This rotation is thought to record a change in local ice-movement direction as the southern part of the Baltic ice stream progressively overrode the Jasmund Peninsula.

During the **fourth stage** (Fig. 15d) the final ice retreat from the Jasmund Peninsula led to a large-scale relaxation in the glacitectonic complex, which was probably accompanied by dewatering of the M1 diamicton. The consistent orientation of S3 in both samples JA03 and JA04 indicates that dewatering of the sediment post-dated the rotation of S1 and S2 during stage 3. The localised reactivation of S2 and southerly directed extension across these R'-type Riedel shears and associated normal faulting within the M1 diamicton are thought to record the late-stage reactivation of the thrust cutting the southwestern limb of the Wissower Bach Syncline due to the gravitational relaxation caused by the retreat of the ice.

The model proposed here to explain the structural development of this syncline involves progressive deformation of the chalk bedrock and glacial sediments during ice advance and subsequent retreat, thereby relating deformation to changes in ice dynamics during the glaciation of the Jasmund Peninsula.

Conclusions

Within the M1 diamicton bounding the main fault (dip to SW/WSW), three different main fabrics were distinguished. The planar S1 fabric (oldest) dips to NW/NE and is split up into the two sub-fabrics S1a (gently inclined) and S1b (steep). S2 is linear and dips to SE/SW (always perpendicular to S1). Here a separation into a steeper and more gently inclined sub-domain (S2a and S2b) could be observed, too. The youngest fabric S3 is nearly vertical, planar and can be interpreted as either steeply inclined shears or anastomosing sub-vertical foliation (dewatering).

The microstructural evolution of the M1 diamicton at the southwestern limb of the Wissower Bach Syncline can be divided into four stages. It starts with an overall sense of compressional movement to the NE (S1, S2) leading to progressive folding (microscale crenulation). This is followed by an anti-clockwise rotation of the microfabric in a narrow shear zone along the tectonic contact between the diamicton and chalk, when the ice partly overrode Jasmund. The evolution ends in dewatering (S3) and a late-stage reactivation (normal faulting due to gravitational relaxation) at the southwestern limb of the Wissower Bach Syncline as the ice retreated.

The results of the present 3D microstructural study, when combined with the macrostructural (field) data, has the potential to provide a more robust dataset on which to interpret the structural evolution of the Wissower Bach Syncline. Moreover, this strategy helps us to better make up the evolutional model of glacitectonic complexes like Jasmund.

Acknowledgements

The Nationalparkamt Vorpommern is thanked for granting the approval to work in the Jasmund National Park. The LiDAR data of Jasmund were provided by the Landesamt für innere Verwaltung – Abt. für Geoinformation, Vermessung und Katasterwesen (LAiV MV) and Jörg Hartleib (Institute for Geography and Geology, University of Greifswald) is thanked for processing the data. We would like to thank Sylvia Weinert (Institute for Geography and Geology, University of Greifswald) for careful preparation of the thin sections. ERP published with the permission of the Executive Director of the British Geological Survey, Natural Environmental Research Council (NERC). Finally, we want to thank Wlodzimierz Narloch (Nicolaus Copernicus University, Torun, Poland), Stig A. Schack Pedersen (GEUS, Copenhagen, Denmark) and David M. Hodgson (University of Leeds, UK) for reviewing and substantially improving this paper.

References

Baroni C, Fasano F. 2006. Micromorphological evidence of warm-based glacier deposition from the Ricker Hills Tillite (Victoria Land, Antarctica). *Quaternary Science Reviews* **25**: 976-992.

Benediktsson ÍÖ, Möller P, Ingólfsson Ó, van der Meer JJM, Kjær KH, Krüger J. 2008. Instantaneous end moraine and sediment wedge formation during the 1890 glacier surge of Brúarjökull, Iceland. *Quaternary Science Reviews* **27**: 209-234.

Benn DI, Evans DJA. 1996. The interpretation and classification of subglacially-deformed materials. *Quaternary Science Reviews* **15**: 23-52.

Bluemle JP, Clayton L. 1984. Large-scale glacial thrusting and related processes in North Dakota. *Boreas* **13**: 279-299.

Burke HF, Phillips ER, Lee JR. 2009. Imbricate thrust stack model for the formation of glaciotectonic rafts: an example from the Middle Pleistocene of north Norfolk, UK. *Boreas* **38**: 620-637.

Credner R. 1892. Rügen. Eine Inselstudie. *Forschungen zur deutschen Landes- und Volkskunde* **7**: 373-494.

Denis M, Guiraud M, Konaté M, Buoncristiani J-F. 2010. Subglacial deformation and water-pressure cycles as a key for understanding ice stream dynamics: evidence from the Late Ordovician succession of the Djado Basin (Niger). *International Journal of Earth Science (Geologische Rundschau)* **99**: 1399-1425.

Fossen H. 2010. *Structural Geology*. Cambridge University Press: New York.

Gripp K. 1947. Jasmund und Möen, eine glacialmorphologische Untersuchung. *Erdkunde* **1**: 175-182.

Grohmann CH, Campanha GAC. 2010. OpenStereo: open source, cross-platform software for structural geology analysis. Presented at the *AGU 2010 Fall Meeting*, San Francisco, CA.

Groth K. 1969. Der glazitektonische Aufbau der Halbinsel Jasmund/Rügen unter besonderer Berücksichtigung der glazidynamischen Entwicklung der Stauchmoräne. *Dissertation, Mathematisch-Naturwissenschaftliche Fakultät, Ernst-Moritz-Arndt-Universität Greifswald*.

Groth K. 2003. Zur glazitektonischen Entwicklung der Stauchmoräne Jasmund/Rügen. *Schriftenreihe des Landesamtes für Umwelt, Naturschutz und Geologie Mecklenburg-Vorpommern* **3**: 39-49.

Harris C, Brabham PJ, Williams GD. 1995. Glaciotectonic structures and their relation to topography at Dinas Dinlle, Arvon, northwest Wales. *Journal of Quaternary Science* **10**: 397.

Harris C, Williams G, Brabham P, Eaton G, McCarroll D. 1997. Glacitectonized Quaternary sediments at Dinas Dinlle, Arvon, North Wales and their bearing on the style of deglaciation in the eastern Irish Sea. *Quaternary Science Reviews* **16**: 109-127.

Hiemstra JF, van der Meer JJM. 1997. Pore-water controlled grain fracturing as an indicator for subglacial shearing in tills. *Journal of Glaciology* **43**: 446-454.

Huuse M, Lykke-Andersen H. 2000. Large-scale glaciotectonic thrust structures in the eastern Danish North Sea. In *Deformation of Glacial Materials* **176**, Maltman AJ, Hubbard B, Hambrey MJ (eds). The Geological Society of London, Special Publication; 293-305.

Jaekel O. 1917. Vier nordische Eiszeiten. *Jahresbericht der Geographischen Gesellschaft Greifswald* **16**: 1-41.

Janke W, Niedermeyer R-O. 2011: Geologische Entwicklung im Pleistozän. In *Die deutsche Ostseeküste*, Niedermeyer R-O, Lampe R, Janke W, Schwarzer K, Duphorn K, Kliewe H, Werner F (eds). Gebr. Borntraeger Verlagsbuchhandlung: Stuttgart; 32-51.

Katzung G, Müller U. 2004. Quartär. In *Geologie von Mecklenburg-Vorpommern*, Katzung G (ed). E. Schweizerbart'sche Verlagsbuchhandlung: Stuttgart; 221-225.

Kenzler M, Tsukamoto S, Meng S, Thiel C, Frechen M, Hüneke H. 2015. Luminescence dating of Weichselian interstadial sediments from the German Baltic Sea coast. *Quaternary Geochronology*, doi: 10.1016/j.quageo.2015.05.015.

Lee JR, Phillips ER. 2008. Progressive soft sediment deformation within a subglacial shear zone – a hybrid mosaic-pervasive deformation model for Middle Pleistocene glaciotectonised sediments from eastern England. *Quaternary Science Reviews* **27**: 1350-1362.

Litt T, Behre K-E, Meyer K-D, Stephan H-J, Wansa S. 2007. Stratigraphische Begriffe für das Quartär des norddeutschen Vereisungsgebietes. *Eiszeitalter und Gegenwart* **56(1/2)**: 7-65.

Ludwig AO. 1964. Stratigraphische Untersuchungen des Pleistozäns der Ostseeküste von der Lübecker Bucht bis Rügen. *Geologie* supplement **42**: 143.

Ludwig AO. 2005. Zur Interpretation des Kliffanschnitts östlich Glowe/Insel Rügen (Ostsee). *Zeitschrift für geologische Wissenschaften* **33(4/5)**: 263-272.

Ludwig AO. 2006. Cyprinenton und I1-Folge im Pleistozän von Nordost-Rügen und der Insel Hiddensee (südwestliche Ostsee). *Zeitschrift für geologische Wissenschaften* **34(6)**: 349-377.

Ludwig AO. 2011. Zwei markante Stauchmoränen: Peski/Belorussland und Jasmund, Ostseeinsel Rügen/Nordostdeutschland – Gemeinsame Merkmale und Unterschiede. *E & G, Quaternary Science Journal* **60/4**: 464-487.

Menzies J. 2000. Micromorphological analyses of microfabrics and microstructures indicative of deformation processes in glacial sediments. In *Deformation of Glacial Materials* **176**, Maltman AJ, Hubbard B, Hambrey MJ (eds). The Geological Society of London, Special Publication; 245-257.

Menzies J, van der Meer JJM, Rose J. 2006. Till – a glacial "tectomict", a microscopic examination of a till's internal architecture. *Geomorphology* **75**: 172-200.

Moran SR, Clayton L, Hooke R LeB, Fenton MM, Andriashek LD. 1980. Glacier-bed landforms of the Prairie Region of North America. *Journal of Glaciology* **25**: 457-476.

Müller U. 2004. Jung-Pleistozän – Eem-Warmzeit bis Weichsel-Hochglazial. In *Geologie von Mecklenburg-Vorpommern*, Katzung G (ed). E. Schweizerbart'sche Verlagsbuchhandlung: Stuttgart; 234-242.

Müller U, Obst K. 2006. Lithostratigraphie und Lagerungsverhältnisse der pleistozänen Schichten im Gebiet von Lohme (Jasmund/Rügen). *Zeitschrift für geologische Wissenschaften* **34**: 39-54.

Narloch W, Piotrowski JA, Wysota W, Larsen NK, Menzies J. 2012. The signature of strain magnitude in tills associated with the Vistula Ice Stream of the Scandinavian Ice Sheet, central Poland. *Quaternary Science Reviews* **57**: 105-120.

Narloch W, Wysota W, Piotrowski JA. 2013. Sedimentological record of subglacial conditions and ice sheet dynamics of the Vistula Ice Stream (north-central Poland) during the Last glaciation. *Sedimentary Geology* **293**: 30-44.

Panzig WA. 1995. Zum Pleistozän Nordost-Rügens. – In *Geologie des südlichen Ostseeraumes – Umwelt und Untergrund*, Katzung G, Hüneke H, Obst K (eds). Terra Nostra, Schriften der Alfred-Wegener-Stiftung **6**: 177-200.

Pedersen SAS. 2000. Superimposed deformation in glaciotectonics. *Bulletin of the Geological Society of Denmark* **46**: 125-144.

Pedersen SAS. 2005. Structural Analysis of the Rubjerg Knude Glaciotectonic Complex, Vendsyssel, northern Denmark. *Bulletin of the Geological Society of Denmark and Greenland* **8**: 1-192.

Pedersen SAS. 2014. Architecture of glaciotectonic complexes. *Geosciences* **4**: 269-296.

Pedersen SAS, Gravesen P. 2009. Structural development of Maglevandsfald: a key to understanding the glaciotectonic architecture of Møns Klint, SE Denmark. *Bulletin of the Geological Survey of Denmark and Greenland* **17**: 29-32.

Phillips ER, Auton CA. 2000. Micromorphological evidence for polyphase deformation of glaciolacustrine sediments from Strathspey, Scotland. In *Deformation of Glacial Materials* **176**, Maltman AJ, Hubbard B, Hambrey MJ (eds). The Geological Society of London, Special Publication; 279-291.

Phillips ER, Evans DJA, Auton CA. 2002. Polyphase deformation at an oscillating ice margin following the Loch Lomond Readvance, central Scotland, UK. *Sedimentary Geology* **149**: 157-182.

Phillips ER, Merritt JW, Auton CA, Golledge NR. 2007. Microstructures developed in subglacially and proglacially deformed sediments: faults, folds and fabrics, and the influence of water on the style of deformation. *Quaternary Science Reviews* **26**: 1499-1528.

Phillips ER, Lee JR, Burke H. 2008. Progressive proglacial to subglacial deformation and syntectonic sedimentation at the margins of the Mid-Pleistocene British Ice Sheet: evidence from north Norfolk, UK. *Quaternary Science Reviews* **27**: 1848-1871.

Phillips ER, Merritt J. 2008. Evidence for multiphase water-escape during rafting of shelly marine sediments at Clava, Inverness-shire, NE Scotland. *Quaternary Science Reviews* **27**: 988-1011.

Phillips ER, van der Meer JJM, Ferguson A. 2011. A new “microstructural mapping” methodology for the identification, analysis and interpretation of polyphase deformation within subglacial sediments. *Quaternary Science Reviews* **30**: 2570-2596.

Phillips, E., Everest, J., Reeves, H. 2012. Micromorphological evidence for subglacial multiphase sedimentation and deformation during overpressurized fluid flow associated with hydrofracturing. *Boreas* **42**: 395–427.

Phillips ER, Lipka E, van der Meer JJM. 2013. Micromorphological evidence of liquefaction, injection and sediment deposition during basal sliding of glaciers. *Quaternary Science Reviews* **81**: 114-137.

Steinich G. 1972. Endogene Tektonik in den Unter-Maastricht-Vorkommen auf Jasmund (Rügen). *Geologie* supplement **71/72**.

Steinich G. 1992. Die stratigraphische Einordnung der Rügen-Warmzeit. *Zeitschrift für geologische Wissenschaften* **20**: 125-154.

Thomas GSP, Chiverrell RC. 2007. Structural and depositional evidence for repeated ice-marginal oscillation along the eastern margin of the Late Devensian Irish Sea Ice Stream. *Quaternary Science Reviews* **26**: 2375-2405.

van der Meer JJM. 1987. Micromorphology of glacial sediments as a tool in distinguishing genetic varieties of till. *Geological Survey of Finland, Special Paper* **3**: 77-89.

van der Meer JJM. 1993. Microscopic evidence of subglacial deformation. *Quaternary Science Reviews* **12**: 553-587.

van der Meer JJM, Menzies J, Rose J. 2003. Subglacial till, the deformable glacier bed. *Quaternary Science Reviews* **22**: 1659-1685.

van der Meer JJM, Kjær KH, Krüger J, Rabassa J, Kilfeather AA. 2009. Under pressure: clastic dykes in glacial settings. *Quaternary Science Reviews* **28**: 708-720.

van der Wateren FM. 1986. Structural geology and sedimentology of the Dammer Berge push moraine, FRG. In *Tills and Glaciotectonics*, van der Meer JJM (ed). Balkema: Rotterdam; 157-182.

van der Wateren FM, Kluiving SJ, Bartek LR. 2000. Kinematic indicators of subglacial shearing. In *Deformation of Glacial Materials* **176**, Maltman AJ, Hubbard B, Hambrey MJ (eds). The Geological Society of London, Special Publication; 259-278.

Vaughan-Hirsch DP, Phillips ER, Lee JR, Hart JK. 2013. Micromorphological analysis of poly-phase deformation associated with the transport and emplacement of glaciotectonic rafts at West Runton, north Norfolk, UK. *Boreas* **42**, 376–394.

von Bülow K. 1955. Stapelmoränen und Untergrund im norddeutschen Jungdiluvium. *Geologie* **4**: 3-14.

Fig. 1 Maps of the investigation area showing **a)** the island of Rügen in the southwestern Baltic Sea adjacent to the North Sea region, **b)** the Jasmund peninsula as the northeastern part of Rügen island, and **c)** the digital elevation model of Jasmund with a separation into the northern and southern structural complex, including the regional ice flow directions and the exact study area Wissower Bach (DEM5, visualised as a hillshade relief model, 10 times vertical exaggeration; data provided by the LAiV MV).

Fig. 2 Panoramic image and geological cross section of the Wissower Bach Syncline. At the southwestern limb of the syncline there is a SW-dipping thrust fault between the Cretaceous chalk and the Pleistocene M1 diamicton below. This area has been sampled for the microstructural analysis of orthogonal thin sections. The abbreviations of the Pleistocene lithostratigraphic units M1, I1, M2, I2 and M3 have been adapted from Jaekel (1917); **a)** tectonic contact between the chalk and the M1 diamicton in detail; **b)** sample blocks JA03 and JA04 at the thrust fault.

Fig. 3 Lower hemisphere stereographic plots showing **a)** the southwestern limb of the Wissower Bach Syncline with an average inclination to SW, **b)** the northeastern limb of the Wissower Bach Syncline dipping to SW, and **c)** the orientation of the thrust fault at the SW limb of the syncline with general dip to SW/WSW; **d)** the structural map illustrates the entire structural conditions at the Wissower Bach.

Fig. 4 Detailed sediment log of the Wissower Bach Syncline with representative photos from selected depositional units. The abbreviations of the Pleistocene lithostratigraphic units M1, I1, M2, I2 and M3 have been adapted from Jaekel (1917). **a)** M3 sediment complex on the top of the cliff comprising the gravel- and boulder-rich channel at the unit's base and the light brown to whitish sandy diamicton. **b)** Lowermost part of the I1 unit starting with the gravel layer at the bottom, which is followed by white to light brown sands. **c)** M1 diamicton at the base of the cliff.

Fig. 5 Microstructures within the M1 diamicton: **a)** round clast alignments without a core stone (JA03.3); **b)** interpreted version (JA03.3); **c)** lineations (JA04.5); **d)** interpreted version (JA04.5); **e)** limestone clast involved in a comet structure (JA03.4); **f)** interpreted version (JA03.4).

Fig. 6 Microstructures within the M1 diamicton and the chalk: **a)** deformed augen structure of the M1 diamicton within the chalk (JA03.1); **b)** interpreted version (JA03.1); **c)** augen-shaped diamicton "clast" in the chalk (JA03.4); **d)** ductile, wavy boundary between the chalk and the diamicton below (JA03.2); **e)** thin chalk veins in the M1 diamicton (JA03.3); **f)** crushed quartz grains in the diamicton (JA04.3).

Fig. 7 Microstructural maps of the thin section JA03.2 showing the tectonic boundary between the chalk on top and the M1 diamicton below. The left map displays the fabrics S1 to S3, including the sub-fabrics of S1 and S2. The right map is the interpretation of the three fabrics. The S1 fabric is locally dislocated by normal faults along the S2 fabric. The rose diagrams illustrate the strength of the individual microfabrics in both depositional units. The northerly inclined fabric in the chalk and the S1 fabric are most dominant.

Fig. 8 Microstructural maps of the thin section JA03.3 showing the tectonic boundary between the chalk on top and the M1 diamicton below. The left map displays the fabrics S1 to S3, including the sub-fabrics of S1 and S2. The right map is the interpretation of the three fabrics. The rose diagrams illustrate the strength of the individual microfabrics in both depositional units. The westerly inclined clast microfabric in the chalk and the S1 fabric are strongly dominant.

Fig. 9 Microstructural maps of the horizontal thin section JA03.6 showing the three fabrics S1 to S3 in the M1 diamicton. The top map displays the fabrics S1 to S3. The bottom map shows the interpretation of the microfabrics. The folded S1 fabric within the microlithons separating the S2 microfabric domains is easily visible. The rose diagram illustrates the strength of the individual microfabrics.

Fig. 10 Microstructural maps of the thin section JA04.1 showing the M1 diamicton. The left map displays the fabrics S1 to S3, including the sub-fabrics of S1 and S2. The right map is the interpretation of the three fabrics. The northerly inclined S1 fabric is dislocated along the southerly inclined S2 fabric ending up in local normal faults. The rose diagram illustrates the strength of the individual microfabrics.

Fig. 11 Microstructural maps of the thin section JA04.3 showing the M1 diamicton. The left map displays the fabrics S1 to S3, including the sub-fabrics of S1 and S2. The right map is the interpretation of the three fabrics. The rose diagram illustrates the strength of the individual microfabrics with the S1 microfabric representing the most dominant one.

Fig. 12 Microstructural maps of the horizontal thin section JA04.5 showing the three fabrics S1 to S3 in the M1 diamicton. The top map displays the fabrics S1 to S3. The bottom map shows the interpretation of the microfabrics. The folded S1 fabric within the microlithons separating the S2 microfabric domains is easily visible. The rose diagram illustrates the strength of the individual microfabrics.

Fig. 13 3D model of the microfabric system at the chalk-diamicton contact (samples JA03, JA04) including the results from the orientation analysis of all thin sections. The lower hemisphere stereographic plots show the orientation of the microfabrics S1, S2 and S3, their shape (linear/planar) and their spatial relationship to each other.

Fig. 14 First suggested model for the Wissower Bach structure developed by the push of an ice stream advancing from NE; **a)** stage 1: ramp thrusting of a chalk sheet over another chalk sheet, directed from NE towards SW; **b)** stage 2: formation of an antiformal stack, probably in the same progressive dynamic event, or alternatively in a readvance of the NE ice.

Fig. 15 Deformational model of the Wissower Bach Syncline including the four evolutional stages; **a)** stage 1: incipient imposition of the large-scale folds which leads to the development of the microfabrics S1 (dip to NE) and S2 (dip to SW) as part of a Riedel shear zone; **b)** second stage with the continuation of large-scale folding and thrusting leading to progressive deformation (crenulation) of S1 and S2 at microscale; **c)** stage 3 comprising the anti-clockwise rotation of the microfabrics S1 and S2 within the narrow shear zone (10 to 20 cm) of the thrust fault presumably by the partial overburden of the glacitectonic complex by the proceeding ice; **d)** stage 4: retreat of the ice and associated relaxation, which ends in local microscale normal-fault movements along the S2 microfabric and dewatering of the M1 diamicton, which produces a ductile deformation of the tectonic boundary and the evolution of the S3 microfabric.

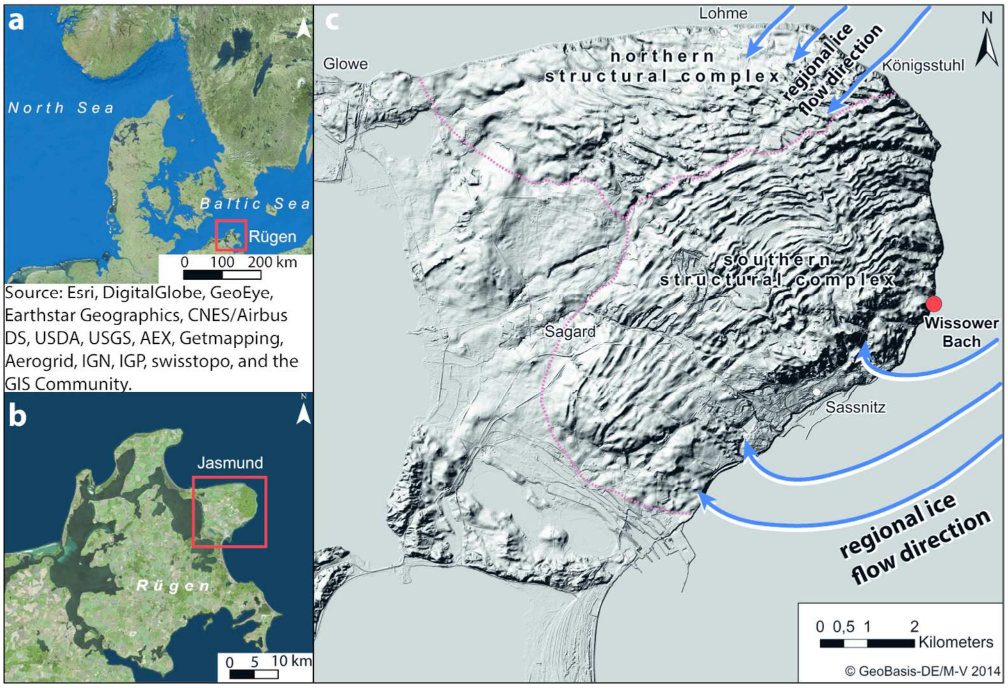

Fig. 1 Maps of the investigation area showing a) the island of Rügen in the southwestern Baltic Sea adjacent to the North Sea region, b) the Jasmund peninsula as the northeastern part of Rügen island, and c) the digital elevation model of Jasmund with a separation into the northern and southern structural complex, including the regional ice flow directions and the exact study area Wissower Bach (DEM5, visualised as a hillshade relief model, 10 times vertical exaggeration; data provided by the LAiV MV).
259x177mm (150 x 150 DPI)

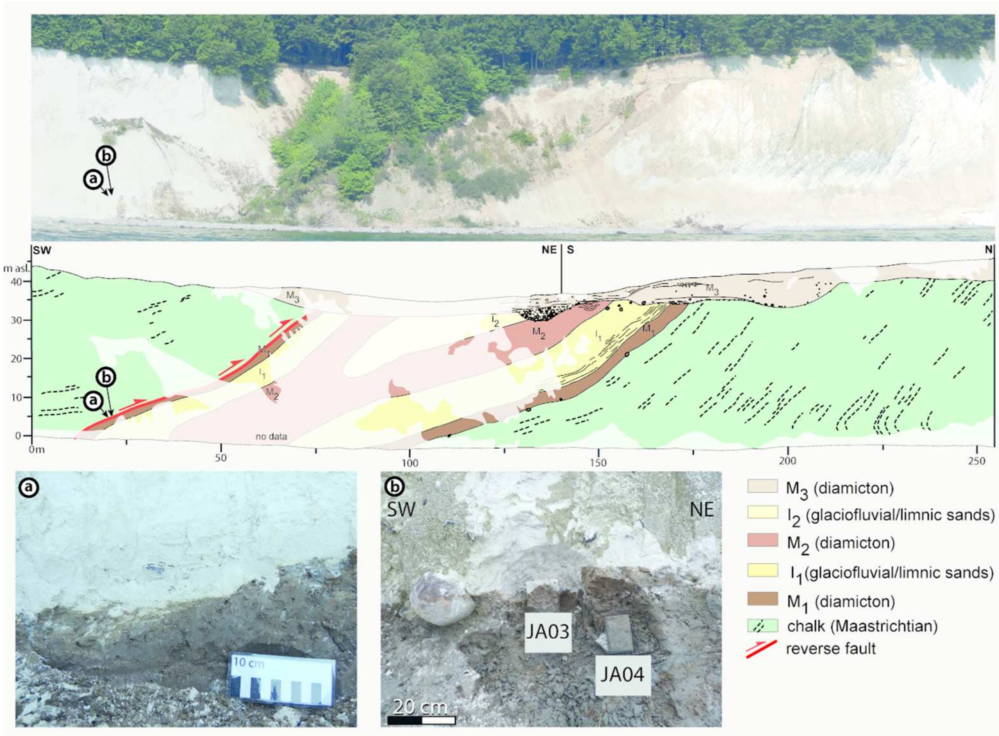

Fig. 2 Panoramic image and geological cross section of the Wissower Bach Syncline. At the southwestern limb of the syncline there is a SW-dipping thrust fault between the Cretaceous chalk and the Pleistocene M1 diamicton below. This area has been sampled for the microstructural analysis of orthogonal thin sections. The abbreviations of the Pleistocene lithostratigraphic units M1, I1, M2, I2 and M3 have been adapted from Jaekel (1917); a) tectonic contact between the chalk and the M1 diamicton in detail; b) sample blocks JA03 and JA04 at the thrust fault.
237x176mm (150 x 150 DPI)

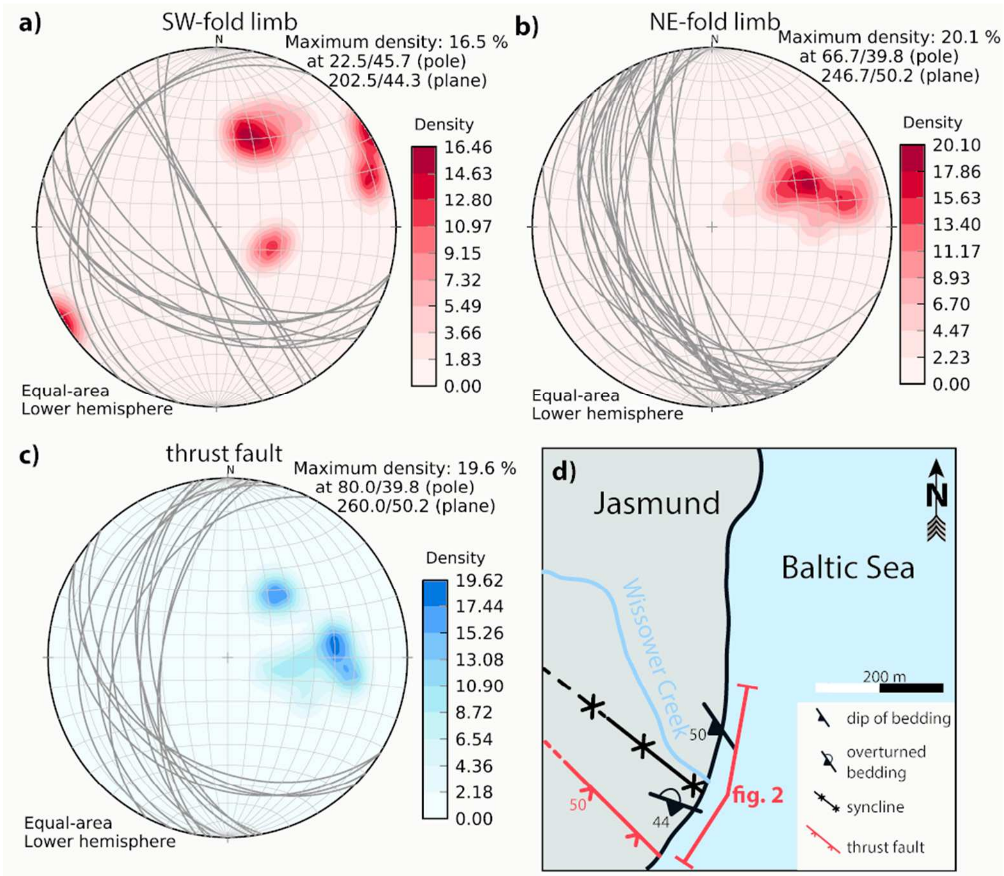

Fig. 3 Lower hemisphere stereographic plots showing a) the southwestern limb of the Wissower Bach Syncline with an average inclination to SW, b) the northeastern limb of the Wissower Bach Syncline dipping to SW, and c) the orientation of the thrust fault at the SW limb of the syncline with general dip to SW/WSW; d) the structural map illustrates the entire structural conditions at the Wissower Bach.

176x154mm (150 x 150 DPI)

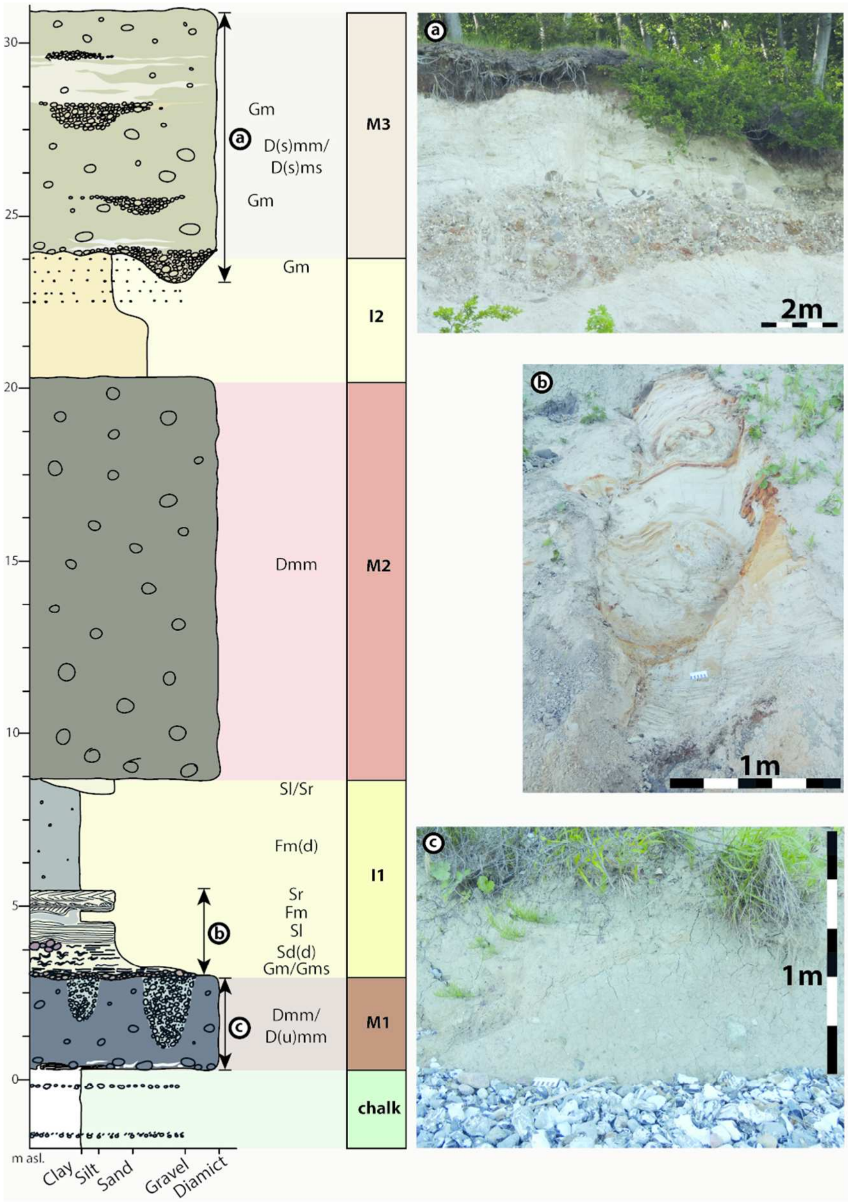

Fig. 4 Detailed sediment log of the Wissower Bach Syncline with representative photos from selected depositional units. The abbreviations of the Pleistocene lithostratigraphic units M1, I1, M2, I2 and M3 have been adapted from Jaekel (1917). a) M3 sediment complex on the top of the cliff comprising the gravel- and boulder-rich channel at the unit's base and the light brown to whitish sandy diamicton. b) Lowermost part of the I1 unit starting with the gravel layer at the bottom, which is followed by white to light brown sands. c) M1 diamicton at the base of the cliff.
176x249mm (150 x 150 DPI)

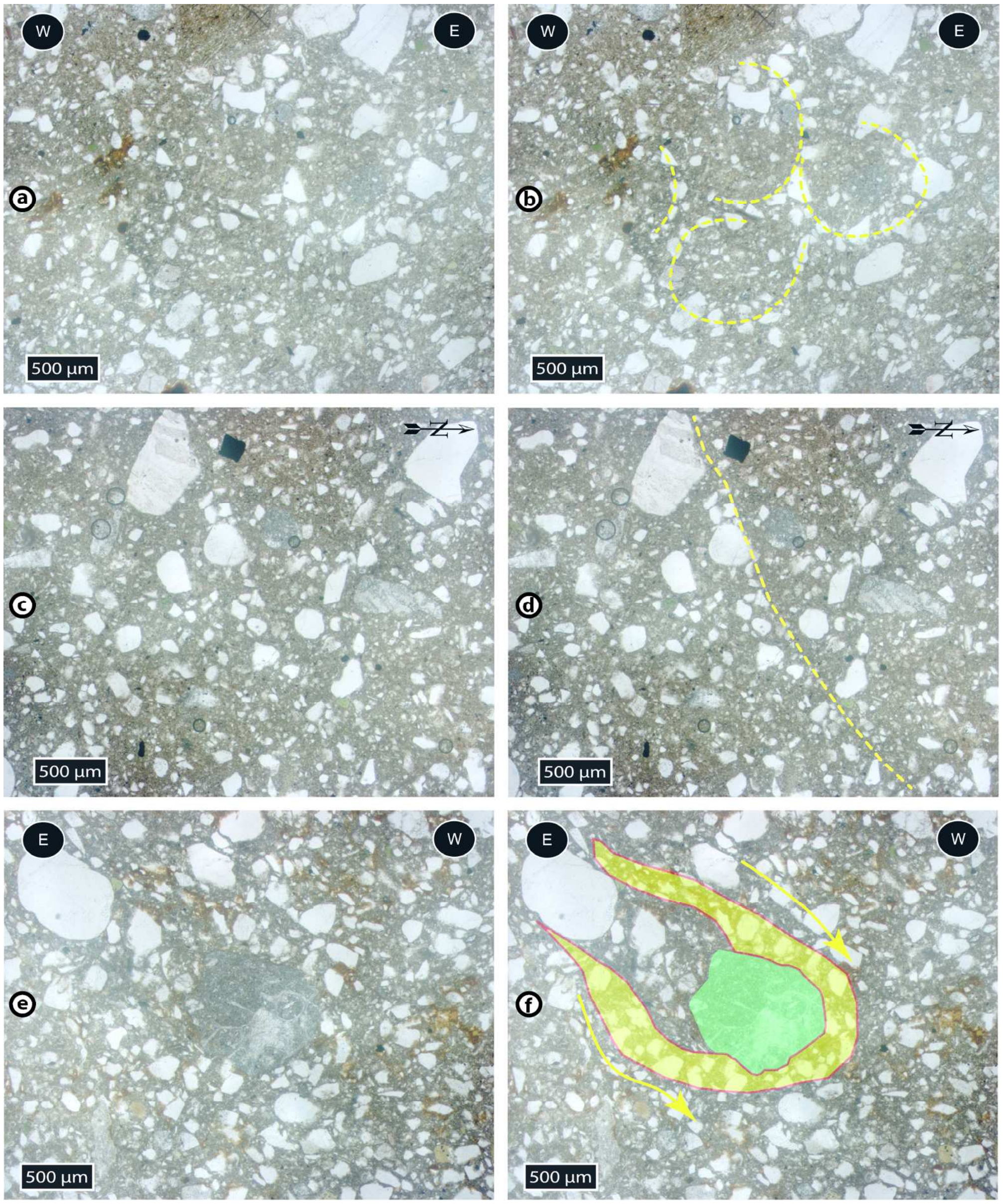

Fig. 5 Microstructures within the M1 diamicton: a) round clast alignments without a core stone (JA03.3); b) interpreted version (JA03.3); c) lineations (JA04.5); d) interpreted version (JA04.5); e) limestone clast involved in a comet structure (JA03.4); f) interpreted version (JA03.4).
176x211mm (300 x 300 DPI)

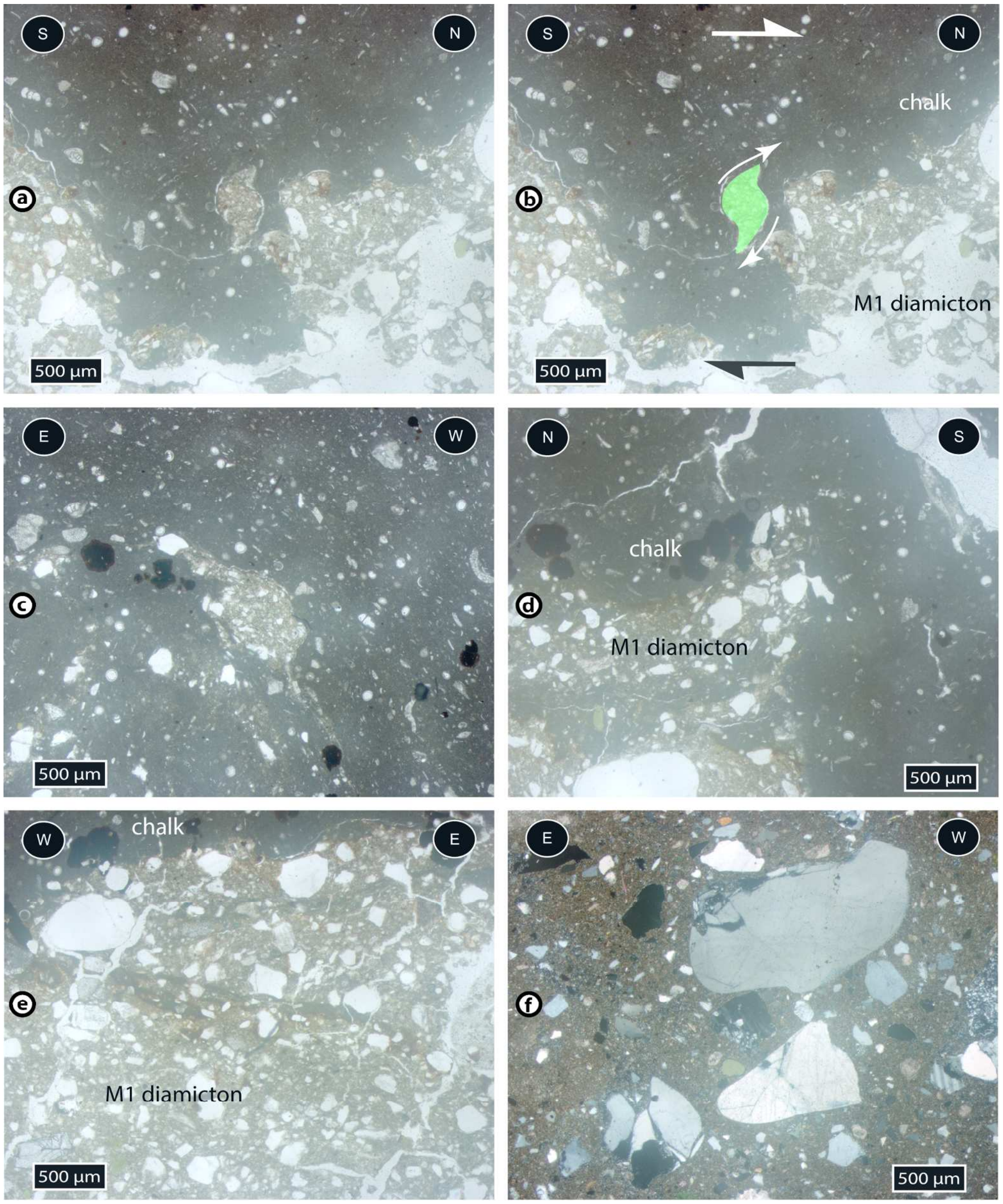

Fig. 6 Microstructures within the M1 diamicton and the chalk: a) deformed augen structure of the M1 diamicton within the chalk (JA03.1); b) interpreted version (JA03.1); c) augen-shaped diamicton "clast" in the chalk (JA03.4); d) ductile, wavy boundary between the chalk and the diamicton below (JA03.2); e) thin chalk veins in the M1 diamicton (JA03.3); f) crushed quartz grains in the diamicton (JA04.3).
176x211mm (300 x 300 DPI)

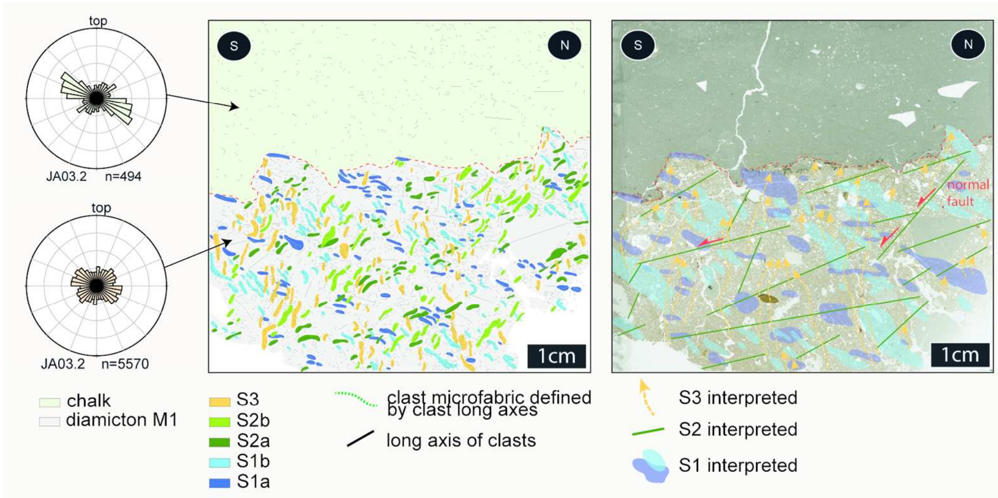

Fig. 7 Microstructural maps of the thin section JA03.2 showing the tectonic boundary between the chalk on top and the M1 diamicton below. The left map displays the fabrics S1 to S3, including the sub-fabrics of S1 and S2. The right map is the interpretation of the three fabrics. The S1 fabric is locally dislocated by normal faults along the S2 fabric. The rose diagrams illustrate the strength of the individual microfabrics in both depositional units. The northerly inclined fabric in the chalk and the S1 fabric are most dominant.
297x149mm (150 x 150 DPI)

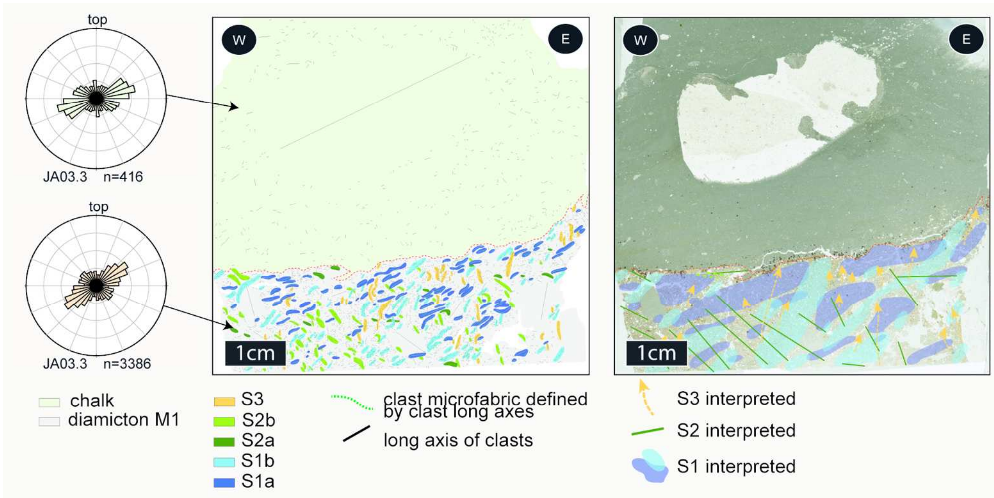

Fig. 8 Microstructural maps of the thin section JA03.3 showing the tectonic boundary between the chalk on top and the M1 diamicton below. The left map displays the fabrics S1 to S3, including the sub-fabrics of S1 and S2. The right map is the interpretation of the three fabrics. The rose diagrams illustrate the strength of the individual microfabrics in both depositional units. The westerly inclined clast microfabric in the chalk and the S1 fabric are strongly dominant.
297x149mm (150 x 150 DPI)

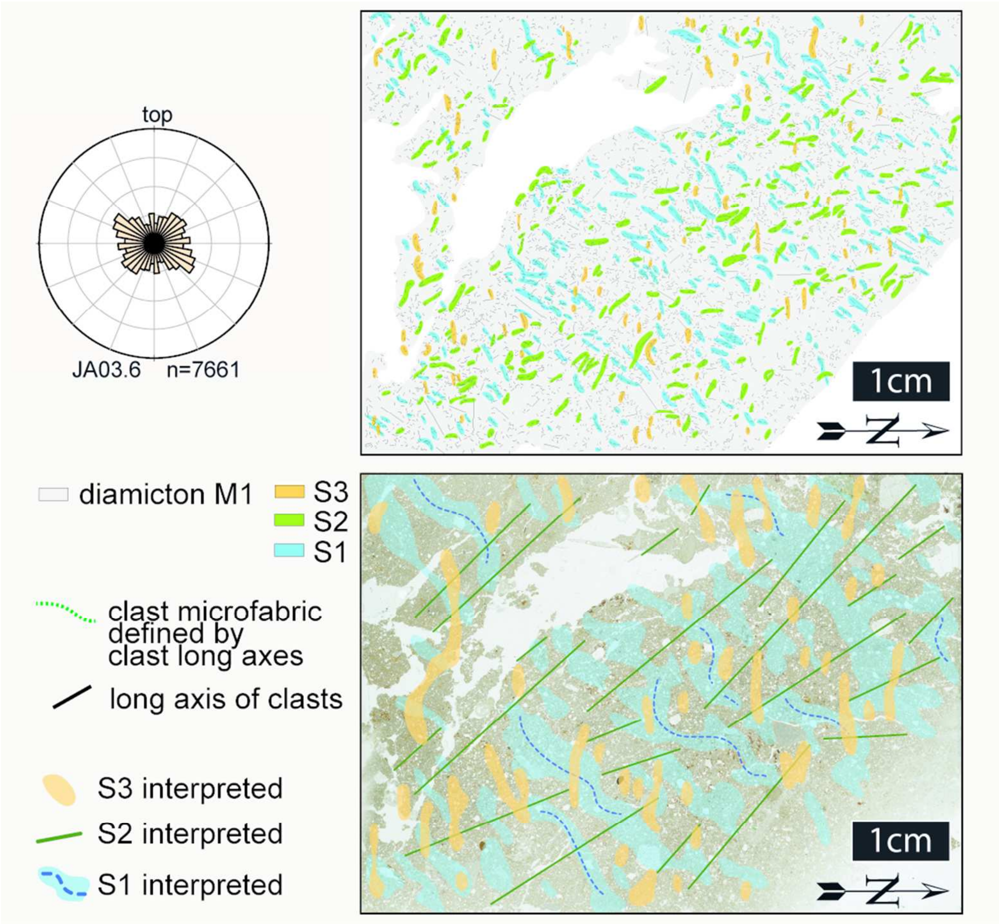

Fig. 9 Microstructural maps of the horizontal thin section JA03.6 showing the three fabrics S1 to S3 in the M1 diamicton. The top map displays the fabrics S1 to S3. The bottom map shows the interpretation of the microfabrics. The folded S1 fabric within the microlithons separating the S2 microfabric domains is easily visible. The rose diagram illustrates the strength of the individual microfabrics.
190x176mm (150 x 150 DPI)

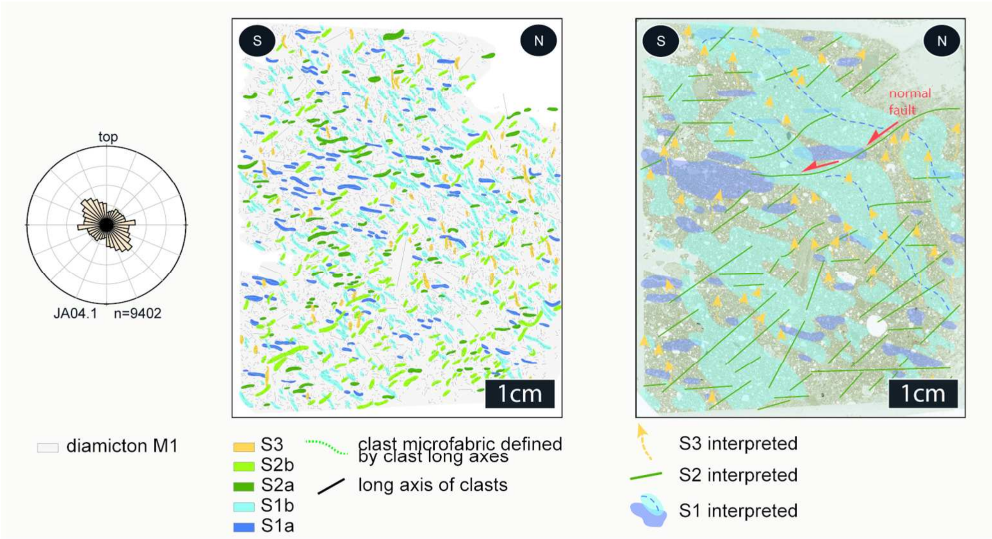

Fig. 10 Microstructural maps of the thin section JA04.1 showing the M1 diamicton. The left map displays the fabrics S1 to S3, including the sub-fabrics of S1 and S2. The right map is the interpretation of the three fabrics. The northerly inclined S1 fabric is dislocated along the southerly inclined S2 fabric ending up in local normal faults. The rose diagram illustrates the strength of the individual microfabrics.
297x161mm (150 x 150 DPI)

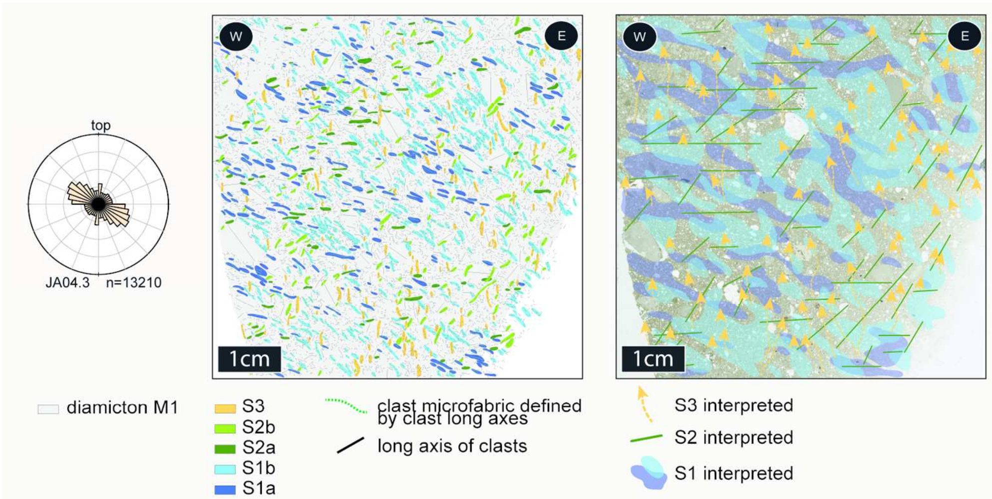

Fig. 11 Microstructural maps of the thin section JA04.3 showing the M1 diamicton. The left map displays the fabrics S1 to S3, including the sub-fabrics of S1 and S2. The right map is the interpretation of the three fabrics. The rose diagram illustrates the strength of the individual microfabrics with the S1 microfabric representing the most dominant one.
297x149mm (150 x 150 DPI)

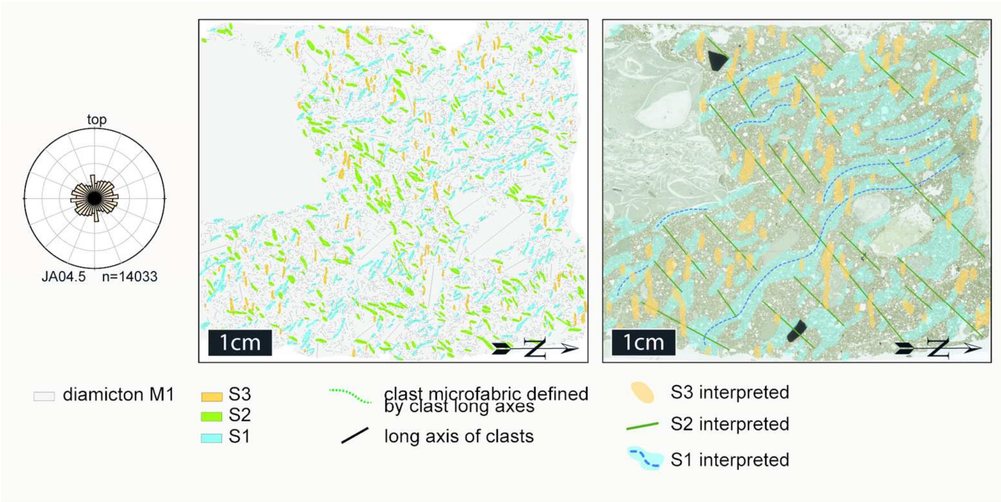

Fig. 12 Microstructural maps of the horizontal thin section JA04.5 showing the three fabrics S1 to S3 in the M1 diamicton. The top map displays the fabrics S1 to S3. The bottom map shows the interpretation of the microfabrics. The folded S1 fabric within the microlithons separating the S2 microfabric domains is easily visible. The rose diagram illustrates the strength of the individual microfabrics.
297x149mm (150 x 150 DPI)

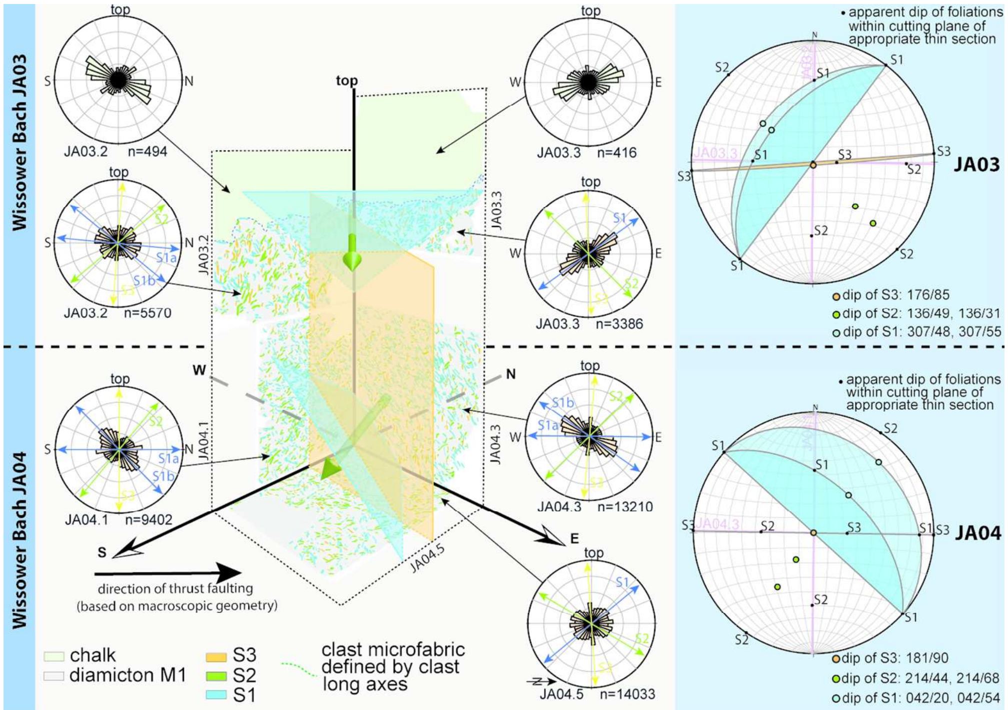

Fig. 13 3D model of the microfabric system at the chalk-diamicton contact (samples JA03, JA04) including the results from the orientation analysis of all thin sections. The lower hemisphere stereographic plots show the orientation of the microfabrics S1, S2 and S3, their shape (linear/planar) and their spatial relationship to each other.
248x175mm (150 x 150 DPI)

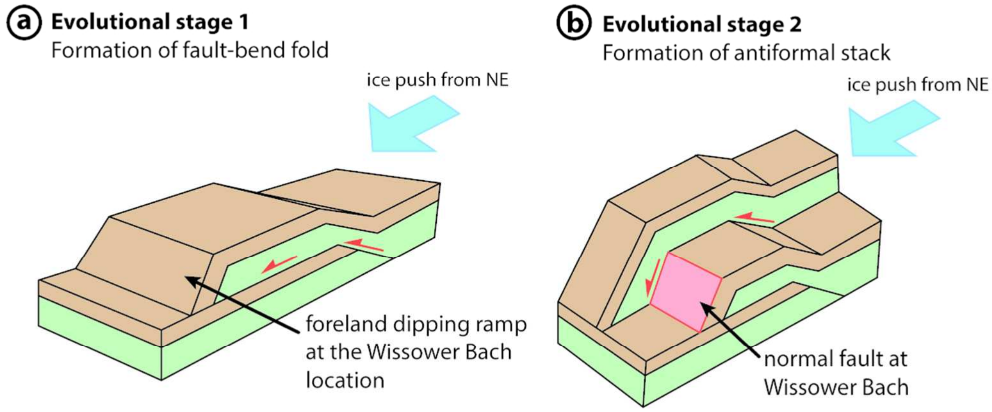

Fig. 14 First suggested model for the Wissower Bach structure developed by the push of an ice stream advancing from NE; a) stage 1: ramp thrusting of a chalk sheet over another chalk sheet, directed from NE towards SW; b) stage 2: formation of an antiformal stack, probably in the same progressive dynamic event, or alternatively in a readvance of the NE ice.
209x93mm (150 x 150 DPI)

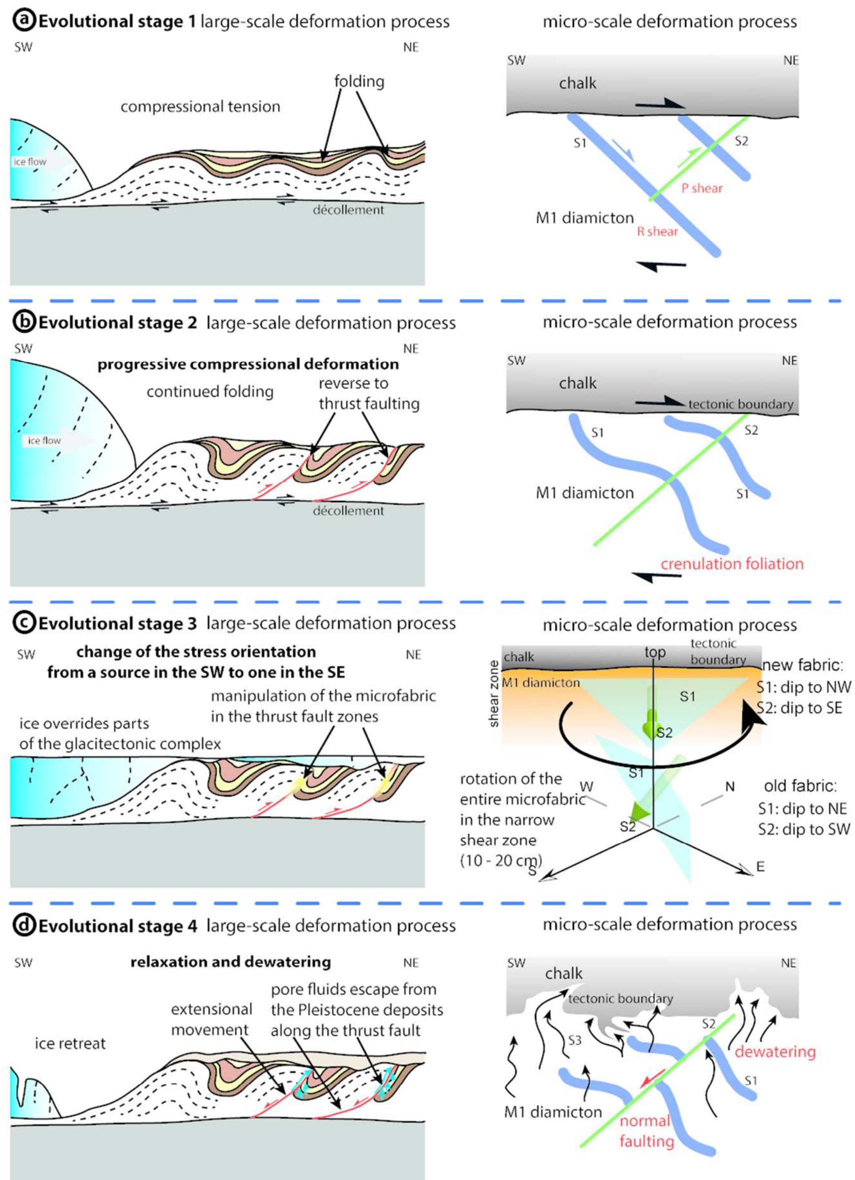

Fig. 15 Deformational model of the Wissower Bach Syncline including the four evolutional stages; a) stage 1: incipient imposition of the large-scale folds which leads to the development of the microfabrics S1 (dip to NE) and S2 (dip to SW) as part of a Riedel shear zone; b) second stage with the continuation of large-scale folding and thrusting leading to progressive deformation (crenulation) of S1 and S2 at microscale; c) stage 3 comprising the anti-clockwise rotation of the microfabrics S1 and S2 within the narrow shear zone (10 to 20 cm) of the thrust fault presumably by the partial overburden of the glacitectonic complex by the proceeding ice; d) stage 4: retreat of the ice and associated relaxation, which ends in local microscale normal-fault movements along the S2 microfabric and dewatering of the M1 diamicton, which produces a ductile deformation of the tectonic boundary and the evolution of the S3 microfabric.
176x247mm (150 x 150 DPI)